Science Translational Medicine
AAAS

stm.sciencemag.org/cgi/content/full/12/553/eabb4757/DC1

Supplementary Materials for

Mapping functional humoral correlates of protection against malaria challenge following RTS,S/AS01 vaccination

Todd J. Suscovich, Jonathan K. Fallon, Jishnu Das, Allison R. Demas, Jonathan Crain, Caitlyn H. Linde, Ashlin Michell, Harini Natarajan, Claudia Arevalo, Thomas Broge, Thomas Linnekin, Viraj Kulkarni, Richard Lu, Matthew D. Slein, Corinne Luedemann, Meghan Marquette, Sandra March, Joshua Weiner, Scott Gregory, Margherita Coccia, Yevel Flores-Garcia, Fidel Zavala, Margaret E. Ackerman, Elke Bergmann-Leitner, Jenny Hendriks, Jerald Sadoff, Sheetij Dutta, Sangeeta N. Bhatia, Douglas A. Lauffenburger, Erik Jongert*, Ulrike Wille-Reece*, Galit Alter*

*Corresponding author. Email: galter@mgh.harvard.edu (G.A.); erik.x.jongert@gsk.com (E.J.); uwille-reece@path.org (U.W.-R.)

Published 22 July 2020, *Sci. Transl. Med.* **12**, eabb4757 (2020)
DOI: 10.1126/scitranslmed.abb4757

The PDF file includes:

Other Supplementary Material for this manuscript includes the following:

(available at stm.sciencemag.org/cgi/content/full/12/553/eabb4757/DC1)

Data file S1 (Microsoft Excel format). Primary data.
Data file S2 (.zip format). Analysis code.

Materials And Methods

Studies, Samples, Antigens, Cell Lines, and Reagents

Study summary

Serum samples were obtained from the following Phase 2a clinical studies of the RTS,S vaccine: NCT01366534 (MAL068) (*14*), NCT00075049 (MAL027) (*15*), and NCT01857869 (MAL071) (*13*). In clinical study NCT01366534, 46 volunteers received a first vaccination of either RTS,S/AS01B or a recombinant adenovirus expressing *P. falciparum* CSP (Ad35.CS.01), followed by two monthly doses of RTS,S/AS01B. In clinical study NCT00075049, 43 volunteers were vaccinated with three doses of RTS,S/AS01B or RTS,S/AS02A at Months 0, 1, and 2. In clinical study NCT01857869, 46 volunteers received three doses of the RTS,S/AS01B vaccine according to a 0-1-2 or 0-1-7 month schedule. The delayed third dose given to participants in the 0-1-7 vaccine arm contained only 20% of the standard vaccine dosage. In all three clinical studies, the vaccines were given intramuscularly to malaria-naïve individuals, who were then were exposed to *P. falciparum* (strain 3D7) via bites from five infected mosquitoes 3 weeks after receiving the final vaccination (*69*). Participants were then monitored for the development of symptoms and treated with chloroquine phosphate if infected. Informed consent was obtained from all participants in these trials.

Samples

For each study, serum samples from two timepoints were analyzed: (1) prior to receiving any vaccination and (2) immediately before the controlled malaria challenge. Experimenters were blinded as to the sample identity until all samples were analyzed and all data had been collected. The use of these samples was deemed “not human research” after review by the Massachusetts General Hospital Institutional Review Board under protocols 2015P001351 and 2017P001927. Additionally, human whole blood and buffy coats were collected at Massachusetts General Hospital from healthy donors who did not participate in the malaria vaccine trials. Use of these internal samples as sources of primary neutrophils, monocytes, and NK cells was similarly deemed “not human research” under protocols 2005P001218 and 2010P002463.

Antigens

Full-length *P. falciparum* CSP was produced in *E. coli* and purified as previously described (*70*). The CSP repeat region peptide NANP6 was chemically synthesized with N-terminal biotin and purified by Genscript. The PfCSP C-terminal peptide Pf16 (EPSDKHIKEYLNKIQNSLSTEWSPCSVTCGNGIQVRIKPGSANKPKDELDYANDIEKKICKMEKCS) (*70*) was chemically synthesized with N-terminal biotin and purified by Biomatik. The CSP repeat region–derived peptide R32LR ($(NVDP(NANP)_{15})_2LR$) (*71*) and Hepatitis B surface antigen (HBsAg) were provided by GlaxoSmithKline. Recombinant influenza HA proteins were purchased from ImmuneTech (#IT-003-001ΔTMp, #IT-003-0011ΔTMp, #IT-003-0042ΔTMp) and used as positive control antigens. Recombinant Ebola glycoprotein (#0501-016) and VP40 protein (#0564-001) were purchased from IBT Bioservices and used as negative control antigens.

Cell lines

The following reagent was obtained through the NIH AIDS Reagent Program, Division of AIDS, NIAID, NIH: CEM.NK^R Cells from Dr. Peter Cresswell (*72, 73*). CEM.NK^R cells were grown in RPMI medium (Sigma, R0883) supplemented with 10% FBS, 2 mM L-glutamine, 10 mM HEPES, 100 IU/ml penicillin, and 100 µg/mL streptomycin (R10). THP-1 cells were purchased from ATCC and grown in R10 medium supplemented with 55 µM β-mercaptoethanol.

Primary and Secondary Antibodies

The following fluorescent antibodies were purchased from BD Biosciences: APC-Cy7 anti-huCD14 (#557831), PE-Cy7 anti-huCD86 (#561128), APC anti-huCD86 (#555660), PE-Cy5 anti-huCD107a (#555802), PE-Cy7 anti-huCD56 (#335791), AF700 anti-huCD3 (#557943), PE anti-huMIP1β (#550078), BV421 anti-huMIP1β (#562900), and FITC anti-huIFNγ (#340449). The following fluorescent antibodies were purchased from BioLegend: Pacific Blue anti-huCD66b (#305112), FITC anti-HLA-DR (#307604), AF700 anti-HLA-DR (#307626), BV605 anti-huCD107a (#328634), APC-Cy7 anti-huCD3 (#300426), and PE anti-huIFNγ (#506507). A FITC-conjugated, goat anti-guinea pig complement C3 polyclonal antibody was purchased from MP Biomedical (#0855385). PE-conjugated secondary antibodies were purchased from Southern Biotech for

the detection of total huIgG (#9040-09), huIgM (#9020-09), huIgA1 (#9130-09), huIgA2 (#9140-09), huIgG1 (#9052-09), huIgG2 (#9070-09), huIgG3 (#9210-09), and huIgG4 (#9200-09).

Systems Serology Assays

Isolation of bulk IgG

Bulk IgG was isolated from human serum samples using the Melon Gel IgG Purification kit (Thermo Fisher, #45212) according to the manufacturer's protocol. IgG was then quantified using a commercially available total human IgG ELISA kit (Invitrogen, #88-50550).

Antigen coupling to fluorescent beads

Yellow-green (#F8823), red (#F8821), and blue (#F8814) 1 µm carboxylate-modified microspheres, as well as 1 µm yellow-green (#F8776) and red (#F8775) NeutrAvidin-labeled microspheres, were all purchased from Thermo Fisher. Magplex-C microspheres were purchased from Luminex Corp. NeutrAvidin-labeled fluorescent microspheres were coupled to biotinylated antigen (1.8×10^8 beads per 5 µg antigen) by co-incubation in PBS/5% BSA (PBSA) overnight at 4°C, then the beads were washed twice with PBSA. Carboxylate-modified, 1 µm fluorescent microspheres (9×10^8 beads per 25 µg antigen) or Magplex-C microspheres (5×10^6 beads per 25 µg antigen) were covalently coupled to antigen using a two-step carbodiimide reaction. Beads were washed and resuspended in 100 mM NaH_2PO_4 (pH 6.2) and activated by incubating with 500 µg Sulfo-NHS (Pierce, #A39269) and 500 µg EDC (Pierce, #A35391) for 30 minutes at room temperature. The beads were washed three times with coupling buffer (50 mM MES, pH 5.0), then incubated with protein antigen in 100 µl of coupling buffer for 2 hours at room temperature. The beads were washed three times with PBS-TBN (1× PBS, 0.1% BSA, 0.02% Tween-20, and 0.05% Sodium Azide, pH 7.4) and blocked with PBS-TBN for 30 minutes at room temperature. Beads were then washed three times with PBS, 0.05% Tween 20, and resuspended in storage buffer (1× PBS, 0.05% Sodium Azide).

Antibody-dependent cellular phagocytosis (ADCP)

A previously described assay was used to measure antibody-dependent phagocytosis by monocytes (*74*). Briefly, 1 µm yellow-green fluorescent beads were coupled to antigen and blocked overnight with PBSA. The

beads were then washed twice with PBSA, diluted to 1.8×10^8 beads/ml, and 10 µl beads/well were added to a 96-well round-bottom microplate (Corning, #7007). Diluted serum from immunized individuals (10 µl/well) was added to the beads and incubated at 37°C for 2 hours to allow the formation of immune complexes. Unbound antibodies were washed off, 25,000 THP-1 monocytes/well were added to the beads in 200 µl THP-1 medium, and the plates were incubated overnight at 37°C. Cells were fixed and acquired on a BD LSRII or Intellicyt iQue Screener PLUS flow cytometer, and data was analyzed using FlowJo (BD) or ForeCyt (Intellicyt) software. The phagocytic score for each sample was calculated using the equation:

$$Phagocytic\ Score\ (PS) = \frac{\%\ bead\text{-}positive\ cells\ \times\ geometric\ mean\ fluoresence\ intensity\ (gMFI)\ of\ bead\text{-}positive\ cells}{10\ \times\ gMFI\ of\ first\ bead\text{-}positive\ peak}$$

For each antigen, pooled seropositive and seronegative samples were titrated in the assay to determine the linear range of the assay, which was used to select the optimal sample dilution. Each serum sample was tested in duplicate.

Antibody-dependent neutrophil phagocytosis (ADNP)

Yellow-green fluorescent beads were coupled to antigen, blocked overnight with PBSA at 4°C, washed twice with PBSA, and diluted to 1.8×10^8 beads/ml. Beads (10 µl beads/well) and diluted serum (10 µl/well) were combined in a round-bottom 96-well plate and incubated at 37°C for 2 hours to allow for immune complex formation. Primary leukocytes were isolated from fresh whole blood collected in anticoagulant citrate dextrose tubes by treatment with ACK red blood cell lysis buffer (Quality Biological, #118-156-101) and diluted to 2.5×10^5 cells/ml in R10. After immune complex formation, the beads were washed, 5×10^4primary leukocytes/well were added, and the plates were incubated for 1 hour at 37°C. Cells were stained for surface CD66b and CD14, fixed, and acquired on a BD LSRII or Intellicyt iQue Screener PLUS flow cytometer. Gates were drawn on SSC^{high} $CD66b^+$ $CD14^-$ cells using FlowJo or ForeCyt software, and phagocytic scores were calculated as described above. For each antigen, pooled seropositive and seronegative samples were titrated in the assay to determine the linear range of the assay, which was used to select the optimal sample dilution. Each serum sample was tested in duplicate.

Antibody-dependent dendritic cell phagocytosis (ADDCP)

Primary immature dendritic cells were generated via the differentiation of primary monocytes into monocyte-derived dendritic cells (MoDCs). Primary monocytes were isolated from PBMCs collected from malaria-naïve individuals using CD14 positive-selection microbeads (Miltenyi, #130-050-201) and grown in vitro for six days in MoDC differentiation medium containing GM-CSF and IL-4 (Miltenyi, #130-094-812). Fluorescent beads were coupled to antigen, blocked with PBSA, washed and diluted to 1.8×10^8 beads/ml. Beads (10 µl beads/well) and IgG purified from the study participants (10 µl of 25 µg/mL IgG/well) were mixed in round-bottom 96-well microplates and incubated at 37°C for 2 hours to allow for immune complex formation. The beads were then washed and added to 4×10^4 primary MoDCs/well in R10 medium, which were then incubated at 37°C for either 4 hours (to assess phagocytosis and cell surface marker expression) or overnight (to assess cytokine production). Plates that were incubated for 4 hours were then stained for surface HLA-DR and CD86, fixed, and acquired on a BD LSRII or Intellicyt iQue Screener PLUS flow cytometer. For acquisition on an LSRII cytometer, antigen-coupled yellow-green fluorescent beads were used, and the cells were stained with AF700 anti-HLA-DR and APC anti-huCD86. For acquisition on the iQue Screener PLUS, antigen-coupled blue fluorescent beads were used, and the cells were stained with FITC anti-HLA-DR and PE-Cy7 anti-huCD86. The phagocytic score for each sample was calculated as described above, and the median fluorescence intensity was reported for each cell surface marker. Supernatants collected from plates that were incubated overnight were mixed with MILLIPLEX cytokine/chemokine magnetic beads (EMD Millipore, #HCYTOMAG-60K) to measure secreted IL-12p40, IL-1β, IL-10, TNFα, IL-6, IFNα2, IP-10, and IL-8. This magnetic bead panel was used according to the manufacturer's instructions, and beads were analyzed with a BioPlex 3D suspension array system (Bio-Rad). Cytokine concentrations were extrapolated from standard curves and reported in units of pg/ml. For all experiments, pooled seropositive and seronegative samples were titrated in the assay to determine the linear range of the assay, which was used to select the optimal sample dilution. Each serum sample was tested using MoDCs isolated from two different donors.

Antibody-dependent complement deposition (ADCD)

Red fluorescent beads were coupled to antigen, blocked with PBSA, washed, and diluted to 1.8×10^8 beads/ml. Beads (10 µl beads/well) and diluted serum (10 µl/well) were combined in a round-bottom 96-well plate and incubated at 37°C for 2 hours to allow or immune complex formation. Guinea pig complement (CedarLane, #CL4051) (*75*) was resuspend per the manufacturer's recommendations and diluted 1:50 in gelatin veronal buffer with calcium and magnesium (GVB++, Boston Bioproducts, #IBB-300). Following immune complex formation, the beads were washed with PBS and incubated with 200 µl diluted complement for 20 minutes at 37°C. The beads were then washed with 15 mM EDTA, stained with FITC-conjugated anti-complement C3, and acquired on a BD LSRII or Intellicyt iQue Screener PLUS flow cytometer. Data were then analyzed using FlowJo or ForeCyt software. Complement deposition was reported as median fluorescence intensity on the FITC channel, after gating on singlet, red fluorescent particles. For each antigen, pooled seropositive and seronegative samples were titrated in the assay to determine the linear range of the assay, which was used to select the optimal sample dilution. Each serum sample was tested in duplicate.

Antibody-dependent NK cell activation (ADNKA)

An ELISA-based assay for measuring antibody-dependent NK cell activation has been described previously (*76, 77*). Briefly, flat-bottom 96-well ELISA plates (Thermo Fisher, #439454) were coated overnight with 100 µl PBS containing 3 µg/ml antigen and then blocked with PBSA. Serum samples from study participants were diluted in PBS, added to the plates, and incubated for 2 hours at 37°C to allow for immune complex formation. Primary human NK cells were purified from buffy coats from healthy donors using the RosetteSep human NK cell enrichment cocktail (StemCell, #15065) and resuspended at 2.5×10^5 cells/ml in R10 media containing 10 µg/ml brefeldin A (Sigma, #B7651), GolgiStop (BD Biosciences, #554724), and fluorescent anti-CD107a. The immune complex–containing ELISA plates were washed three times with PBS, 200 µl NK cells per well were added, and the plates were incubated at 37°C for 5 hours. The cells were then stained for surface CD56 and CD3, fixed and permeabilized (Thermo Fisher, #GAS-003), stained with fluorescent antibodies to IFN-γ and MIP-1β, and acquired on a BD LSRII or Intellicyt iQue Screener PLUS flow cytometer. For acquisition on an LSRII, cells were stained with PE-Cy7 anti-huCD56, AF700 anti-huCD3, PE-Cy5 anti-huCD107a, PE anti-

huMIP-1β, and FITC anti-huIFNγ. For acquisition on an iQue Screener PLUS, cells were stained with PE-Cy7 anti-huCD56, APC-Cy7 anti-huCD3, BV605 anti-huCD107a, BV421 anti-huMIP-1β, and PE anti-huIFNγ. Gates were drawn on singlet, $CD56^+/CD3^-$ cells using FlowJo or ForeCyt software, and the results were reported as the percentage of NK cells that expressed surface CD107a, intracellular MIP-1β, or intracellular IFN-γ. For all experiments, pooled seropositive and seronegative samples were titrated in the assay to determine the linear range of the assay, which was used to select the optimal sample dilution. Each serum sample was tested using NK cells isolated from at least two different donors.

Antibody-dependent cellular cytotoxicity (ADCC)

A previously described rapid fluorometric antibody-dependent cellular cytotoxicity (RFADCC) assay was used to measure ADCC activity (*78*). Briefly, CEM.NK^R cells were incubated with full-length PfCSP antigen in serum-free RPMI for 1 hour at room temperature and then washed twice in RPMI. The antigen-pulsed CEM.NK^R cells were then labeled with the fluorescent dyes CFSE (Invitrogen, #C1157) and PKH26 (Sigma, #MINI26-1KT) according to the manufacturers' instructions. The stained cells were then washed and incubated in V-bottom 96-well microplates (1×10^4 cells per well) with IgG purified from study participants (2.5 µg per well) for 15 minutes at 37°C. Primary human NK cells were purified from buffy coats of seronegative donors using the RosetteSep Human NK Cell Enrichment Cocktail (StemCell) and added to the target cells at an effector-to-target cell ratio of 10:1. The plates were incubated at 37°C for 5 hours, and the cells were then fixed and acquired on a BD LSRII or Intellicyt iQue Screener PLUS flow cytometer. To identify CEM.NK^R target cells, a gate was drawn on PKH26-positive cells. Fluorescent dye-labeled CEM.NK^R cells that were not incubated with NK cells were used to set a gate for CFSE-positivity. Target cell lysis was calculated using the equation:

$$Percent\ lysis = \frac{\#\ PKH26^+\ CEM.NK^R\ cells\ with\ reduced\ CFSE}{\#\ PKH26^+\ CEM.NK^R\ cells} \times 100$$

CEM.NK^R target cells that were labeled with CFSE and PKH26 but were not incubated with CSP antigen were used as a negative control for every test sample to confirm that the responses observed were CSP specific. Pooled seropositive and seronegative samples were titrated in the assay to determine the linear range of the

assay, which was used to select the optimal sample dilution. Each serum sample was tested using NK cells isolated from at least two different donors.

Antigen-specific antibody isotype and subclass analysis

The isotypes and subclasses of antigen-specific antibodies were quantified using a previously described method (*79*). Briefly, Luminex beads were coupled to PfCSP, HBsAg, influenza hemagglutinin (HA), Ebola glycoprotein (GP), or streptavidin via carbodiimide crosslinking with Sulfo-NHS and EDC. Streptavidin-coupled beads were then incubated overnight with biotin-conjugated NANP6 or Pf16 peptide. Each antigen was coupled to a different Luminex bead region, the beads were blocked with PBSA, and then all of the bead regions were pooled and added to black flat-bottom 384-well plates (Greiner Bio-One, #781906) so that each well contained 1500 beads of each region. Serum from study participants was diluted in PBSA and added to the beads, and the plates incubated for 2 hours at room temperature with shaking (800 rpm). The beads were washed three times with wash buffer (1×PBS, 0.1% BSA, 0.5% Triton X-100), then incubated with a PE-conjugated antibody to detect total IgG, IgG1, IgG2, IgG3, IgG4, IgM, IgA1, or IgA2 for 2 hours at room temperature with shaking (800 rpm). The beads were then washed, resuspended in sheath fluid, and acquired on a Bio-Rad BioPlex 3D suspension array system or Intellicyt iQue Screener PLUS flow cytometer. Results were reported as the median PE fluorescence intensity for each antigen-coupled bead region. Pooled seropositive and seronegative samples were titrated in the assay to determine the linear range of the assay, which was used to select the optimal sample dilution. Each serum sample was tested in duplicate.

Antigen-specific antibody Fc receptor binding

The ability of antigen-specific antibodies to bind to human Fc receptors and complement C1q was measured using an assay described previously (*80, 81*). Briefly, avi-tagged FCGR2A(H), FCGR2A(R), FCGR2B, FCGR3A(V), FCGR3A(F), and FCGR3B proteins were produced and purified by the Duke Human Vaccine Institute Protein Production Facility. These proteins were then biotinylated with BirA ligase using a commercially available kit (Avidity, #BirA500). Purified human C1q protein (MP Biomedical, #021913910) was biotinylated using EZ-Link Sulfo-NHS-SS-Biotin (Pierce, #21331). Excess biotin was removed by diluting the FcRs and C1q with PBS and concentrating them with a 3 kDa-cutoff centrifugal filter unit (Amicon,

#UFC500324). These biotinylated Fc domain-binding proteins were then incubated at a 4:1 molar ratio with streptavidin-PE (Prozyme, #PJ31S) for 10 minutes and finally blocked with 5 µM free biotin to generate the assay detection reagents. Luminex beads were coupled to PfCSP, NANP6, Pf16, HBsAg, influenza HA, and Ebola GP antigens as described above. Each antigen was coupled to a different Luminex bead region, the beads were blocked with PBSA, and then all of the bead regions were pooled and added to black flat-bottom 384-well plates so that each well contained 500 beads of each region. These antigen-coupled beads were then combined and incubated with diluted sera from study participants for 2 hours at room temperature with shaking. The beads were then washed and incubated with 1 µg/ml of one of the PE/FcR conjugates for 1 hour at room temperature on a plate shaker. The beads were washed again, resuspended in xMAP sheath fluid (Luminex Corp., #40-75680) and acquired on a BioPlex 3D instrument (Bio-Rad). Results are reported as the median PE fluorescence intensity for each bead region Pooled seropositive and seronegative samples were titrated in the assay to determine the linear range of the assay, which was used to select the optimal sample dilution. Each serum sample was tested in duplicate.

Antigen-specific Fc glycan analysis

The Fc glycans on antigen-specific IgG were analyzed using a previously described method (*82, 83*). Briefly 200 µl of serum from each study participant was heat-inactivated at 56°C for 1 hour and centrifuged at 20,000×g for 10 minutes at room temperature. The resulting supernatant samples were pre-cleared by incubating with 1 µm magnetic streptavidin-coated microspheres (New England Biolabs, #S1420S) for 1 hour at room temperature. A magnet was used to pellet the beads, and the supernatants were then transferred to new tubes containing beads that had been coupled to biotinylated Pf16 peptide. The samples and Pf16-coupled beads were incubated for 1 hour at 37°C with rotation. The beads were then pelleted again, and the supernatants were transferred to new tubes containing beads coupled to biotinylated NANP6 peptide. The samples and NANP6-coupled beads were incubated for 1 hour at 37°C with rotation, the beads were pelleted, and the supernatant was discarded. The Pf16- and NANP6-coupled beads were then washed three times with buffer (0.5 M NaCl, 20 mM Tris-HCl (pH 7.5), 1 mM EDTA), resuspended in PBS, and incubated with IdeZ enzyme (New England Biolabs, #P0770S) for 1 hour at 37°C to cleave the Fc fragments from the antibody-bound beads. These Fc

fragments were transferred to new tubes and incubated with PNGase F (Applied Biosystems, #A28404) for 1 hour at 50°C to remove the glycans from the Fc fragments. The glycans were then isolated and labeled with APTS dye using a GlycanAssure kit (Thermo Fisher, #A28676) according to the manufacturer's instructions. Finally, APTS-labeled glycan samples were analyzed by capillary electrophoresis on an ABI 3500xL Genetic Analyzer. Peaks were assigned based on the migration of known standards (Prozyme, #GKSP-520). The area under the peak for each Fc glycan structure was calculated using GlycanAssure data analysis software. Samples were analyzed in singlicate, and results are reported as the relative proportion of a particular glycan structure within a given sample.

Systems Serology Data Analysis and Visualization

Basic data analysis and visualizations were performed within the Matlab statistical computing environment (supported by the Statistics and Optimization toolboxes). Network visualizations were performed using Cytoscape (*84*).

Classification of vaccine arms for the MAL068 trial

Classification models were trained to distinguish individuals between the two vaccination arms—RRR and ARR—based on the measured humoral immune responses. Models were built using an approach similar to one described previously (*85*): a combination of the least absolute shrinkage and selection operator (LASSO) (*86*) for feature selection and then classification using the LASSO-selected features. The set of model inputs comprised functional and biophysical humoral responses to the full-length CSP protein, the NANP6 peptide and the Pf16 peptide.

The robustness of the model was evaluated using tenfold cross validation replicates. For each tenfold cross validation run, individuals were randomly divided into ten subsets. This was done such that for each fold, nine subsets served as the training set, and the tenth one served as the test set. Each subset served as the test set once. Thus, for each cross-validation run, each individual was in the test fold exactly once. For each such fold, LASSO-based feature selection was performed using the nine subsets designated as the training set for that fold. The coefficient for the LASSO penalty term (i.e., lambda for regularization) was determined via a second

internal tenfold cross validation using only the fold-specific training dataset. Thus, the lambda for regularization can be different for every fold. A fold-specific support vector machine (SVM) (*87*) classifier (linear kernel with default Matlab parameters) was trained using the LASSO-selected features and training data for that fold. This fold-specific classifier was then used to predict labels for the individuals in the test set for that fold. This process was performed for each of the ten folds. Thus, at the end of each cross-validation run, we obtain a set of predicted arm labels for each individual. We performed 20 independent tenfold cross-validation replicates, to account for different ways in which the training and test folds can be split. This is a stringent and appropriate way of performing cross-validation, as both steps involved in the model (feature selection and subsequent classification using the selected features) are performed in a cross-validation setting with data held out. We also report visualizations of the first two latent variables (LVs) from a partial least square discriminant analysis (PLSDA) model trained on the LASSO-selected features (*85*). Rather than being directly measured in our assays, LVs are composite variables composed of the LASSO-selected features that are inferred through mathematical modeling.

The significance of model performance was measured using two independent "negative control" approaches. The repetitions of tenfold cross-validation generated a distribution of model classification accuracies. Corresponding model accuracy distributions were generated for two negative control models. The approach was using permutation testing (*88*), by randomly shuffling the data with respect to the arm labels, within the cross validation framework described above (thus a cross-validation framework matched to the actual model). The features themselves were not shuffled, preserving the correlation structure of the data. The second approach used, within a cross-validation framework, randomly selected size-matched subsets of features. Here too, the correlation structure of the data was preserved. For each control model approach, these processes were repeated 100 times to generate a distribution of model accuracies observed in the context of permuted data and randomly selected size-matched feature sets.

The entire procedure was repeated across all ten cross-validation folds. After running through all ten folds, we compared the predicted arm label for each individual (each individual was in the test set in exactly one of the ten cross validation folds) to the true arm labels, and obtained a true classification accuracy (equivalent to

average classification accuracy across the folds, as the folds are of equal size). We computed the *P* value as the tail probability of the true classification accuracy in the distribution of control model classification accuracies. We reported median *P* values across the independent cross validation replicates.

To evaluate the effectiveness of the PLSDA-based visualization on the LASSO-selected features, we compared the distributions of each of the individual LASSO-selected features as well as LV1 (latent variable 1 from the PLSDA model) across the two vaccination arms. LV1 summarizes the individual selected features into a composite variable that best explains the differences across the groups of interest (e.g. protected and infected individuals). The significance of each comparison was assessed using a Mann-Whitney test *P* value. The *P* value for LV1 was more significant than the P values for any of the individual LASSO-selected features.

Classification models of protection for the MAL068 trial

Overall and arm-specific models of protection were also built using a LASSO approach similar to that described above for arm classification. Separate models were built for each of the three scenarios – 1) all individuals from the RRR and ARR arms combined, 2) individuals only from the RRR arm, 3) individuals only from the ARR arm. The target variable was protection – i.e., whether the individual was protected from infection. The performance of each model was measured in a tenfold cross-validation framework, analogous to what has been described above. The significance of the models was assessed by comparing the real models to the "negative control" models, based on either permuted data or randomly selected features, as described above (in the arm classification section). *P* values were computed using permutation tests, as described in the arm classification section.

To visualize the LASSO-selected features in two dimensions, we used a PLSDA model trained on the LASSO-selected features. The effectiveness of this visualization was assessed as described above. For each of the 3 models of protection, the *P* value for LV1 was more significant than the P values for any of the individual LASSO-selected features.

Correlation networks

We constructed correlation networks centered around 1) the features that stratified arms and 2) the correlates of protection, as previously described (*85*). Briefly, Spearman correlations between all pairs of features were computed and the significance of the correlations was assessed using the false discovery rate (post Benjamini-Hochberg multiple testing correction). A correlation was defined as significant only if it passed both an effect size threshold (those with $|r| > 0.7$) and a statistical significance threshold (FDR <0.01). This is a stringent way to define significant correlations and allows one to focus on the most robust correlations. These significant correlations were visualized as a network.

Prediction across vaccine trials

First, to evaluate the predictive power of the correlates identified from the RRR arm of the MAL068 trial, we built an SVM model using these correlates, and only data from the RRR arm of the MAL068 trial. We then used this model to predict protection for a) the "3× standard RTS,S dose" arm in the MAL027 trial and b) the "3× standard RTS,S dose" arm in the MAL071 trial. In both cases, performance was measured in terms of area under the receiver operating characteristic curve (AUROC). This provides the most stringent evaluation framework for cross-prediction across vaccine trials as both 1) correlate identification and 2) model building were done using data only from the RRR arm of the MAL068 trial i.e., no data from the MAL027 or MAL071 trials were used for either correlate identification or model training. Exact P values are computed to estimate the significance of the AUROC. Specifically, the P value is calculated as the tail probability of the true model performance in a distribution of "null" (control) model performances. A distribution of null model performances is computed using permutation testing i.e., permuting/shuffling the true outcome labels with regard to the data. In each case described above, model training and evaluation are done using completely independent datasets, allowing the most stringent benchmarking of the relevant immune correlates.

When reporting AUCs for single/individual features, we compute the predictive power of the raw data for that feature in stratifying based on outcome (protected or infected). This is theoretically equivalent to the Mann-Whitney U test P value for that feature and measures how good that individual feature is in terms of stratifying

based on outcome. Confidence intervals (75%) for AUC were estimated using 200 bootstrap replicates (normal approximated interval with bootstrapped bias and standard error).

Cross-prediction analyses for predicting time-to-infection values were performed analogously. Here too, model construction and evaluation were using independent datasets; the model used correlates identified from MAL068 and was trained using only MAL068 time-to-infection data. This was then used to predict time-to-infection values for MAL027 and MAL071. Significance of model performance was evaluated using Spearman correlations between true and predicted time-to-infection values.

In vitro antibody-dependent, NK cell–mediated sporozoite restriction

Parasites

P. falciparum sporozoites were freshly purified from mosquito salivary glands by dissection. Briefly, infected female mosquitoes were anaesthetized at -20°C for 5 min and then decapitated. Salivary glands of individual decapitated females were collected in a small volume of Schneider's Insect medium and disrupted using a disposable pestle in a cell strainer. Free sporozoites in 10 µl were counted using a disposable hemocytometer at 100× magnification using a Nikon Eclipse TE200 microscope. Sporozoites were kept on ice and used within 1 hour of dissection. For SEM experiments, cryopreserved *P. falciparum* sporozoites (*89, 90*) were thawed at 37°C for 30 seconds, then reconstituted in 200 µl of assay media warmed to 37°C. Cryovials were centrifuged at 13,000 rpm for 2 minutes, washed, and resuspended in assay media, and used immediately.

P. falciparum infection

Cryopreserved human hepatocytes (BioReclamation IVT) were thawed and seeded onto micropatterned 24 well plates as previously described (*43*). Between 12 and 24 hours after hepatocyte seeding, NK cells freshly isolated from healthy human donors using the RosetteSep NK Cell Enrichment Kit (StemCell Technologies) were added to transwells (Corning 3.0 µm filter) above the micropatterned hepatocytes in a 24 well plate. Freshly isolated sporozoites (3×10^5) were incubated with 10 µg/ml antibodies for 10 minutes at room temperature and added to

the transwell with the NK cells. The plates were incubated at 37°C for 20 minutes, centrifuged at 3000 rpm for 5 minutes, and incubated at 37°C for 3 hours before analysis via immunofluorescence.

PfCSP double-stained immunofluorescence entry assay

Following incubation, transwells were removed and discarded, and plates were fixed in 4% PFA for 20 minutes at room temperature (3 hours post-invasion timepoint). Cells were double-stained with a *P. falciparum* CSP-specific monoclonal antibody (clone 2A10), following a previously described method (*43*). Briefly, cells were blocked in 2% BSA in PBS for 30 minutes, then incubated with 10 µg/ml PfCSP-specific monoclonal antibody (clone 2A10) in blocking buffer for 1 hour at room temperature. After washing, cells were incubated with AlexaFluor 488–conjugated goat anti-mouse secondary for 1 hour at room temperature. Following incubation, the cells were washed again in PBS, permeabilized in ice-cold methanol for 10 minutes at 4°C, and washed again. The staining steps outlined above were then repeated on the permeabilized cells except an AlexaFluor 594–conjugated goat anti-mouse secondary antibody was used. The stained cells were counterstained with Hoechst and mounted in AquaMount mounting media. The samples were imaged at 20× magnification on a Nikon Eclipse Ti-E fluorescence microscope with Andor Zyla sCMOS camera. Three wells were counted per condition using Acumen Explorer with a minimum of 100 events scored per well.

Scanning Electron Microscopy

Sporozoites ($1–2×10^5$) were incubated 5–10 minutes with 10 µg/ml antibody at room temperature, then deposited on 0.1% poly(L-Lysine)-coated coverslips or glass slides with an equal number of NK cells freshly isolated from healthy human donors using RosetteSep NK Cell Enrichment Kit (StemCell Technologies). The cells and sporozoites were incubated for 1 hour at 37°C and fixed in 2% glutaraldehyde/0.1M sodium cacodylate for 1 hour at 4°C. After washing, the cells/sporozoites were subsequently fixed again in 1% Osmium Textroxide for 30 minutes at 4°C. The slides were washed again and dehydrated with increasing concentrations of ethanol. After dehydration, the slides were immersed in increasing concentrations of tetramethylsilane and air dried at room temperature. Finally, the samples were coated in gold, and imaging was performed on a Zeiss Crossbeam 540 Scanning Electron Microscope.

In vivo sporozoite restriction

Molecular cloning, production, and purification of mAbs

The CSP repeat-specific human IgG1 mAbs 250, 311, and 317 (*42*) as well as the isotype control mAb 1245 (*91*) were produced and purified by LakePharma. In addition, DNA fragments encoding the mAb 311 variable heavy chain, the human IgG1 Fc domain (wild-type and N297Q variant sequences), the furin P2A sequence, and the mAb 311 variable light chain were synthesized with flanking BsaI cleavage sites using an SGI-DNA BioXP 3200 system and cloned into separate pUC vectors. Two mAb 311 expression constructs (one with a wild-type huIgG1 Fc and one with an N297Q variant) were then generated by digesting the pUC plasmids with BsaI-HFv2 (New England Biolabs, #R3733) and ligating the inserts into a pDEST vector containing the human lambda light chain sequence. These expression constructs (0.5mg DNA/ml) were transfected separately into suspension 293F cells (1.2×10^6 cells/ml, grown in Gibco FreeStyle 293 Expression Media) using 1.5 ml PEI/ml (polyethylenimine, Polysciences #23966). Supernatants were harvested 5 days later and incubated overnight at 4°C with Protein A/G Plus Agarose (Pierce, #20423). The supernatants were then poured over Chromatography Econo-Columns (Bio-Rad) to collect the agarose resin. The resin was washed with PBS before antibody was eluted with IgG Elution Buffer (Pierce, #21028) into tubes containing 1/10 volume Tris-HCl solution (pH 8.0).

Mouse malaria challenge study

Female C57BL/6 mice were purchased from Charles River Laboratories and used according to animal study protocol MOI7H369, which was approved by the ACUC at Joh Hopkins University. Mice (6–7 weeks old) were injected i.v. with 25 mg purified anti-CSP or control mAb. Sixteen hours later they were injected i.v. with 2×10^3 *P. berghei* sporozoites expressing *P. falciparum* CSP and GFP-luciferase (*91*). Forty-two hours after sporozoite challenge, mice were injected i.p. with 100 μl of D-luciferin (30 mg/mL), anesthetized with isoflurane, and imaged with an IVIS Spectrum system to measure the bioluminescence expressed by the chimeric parasites.

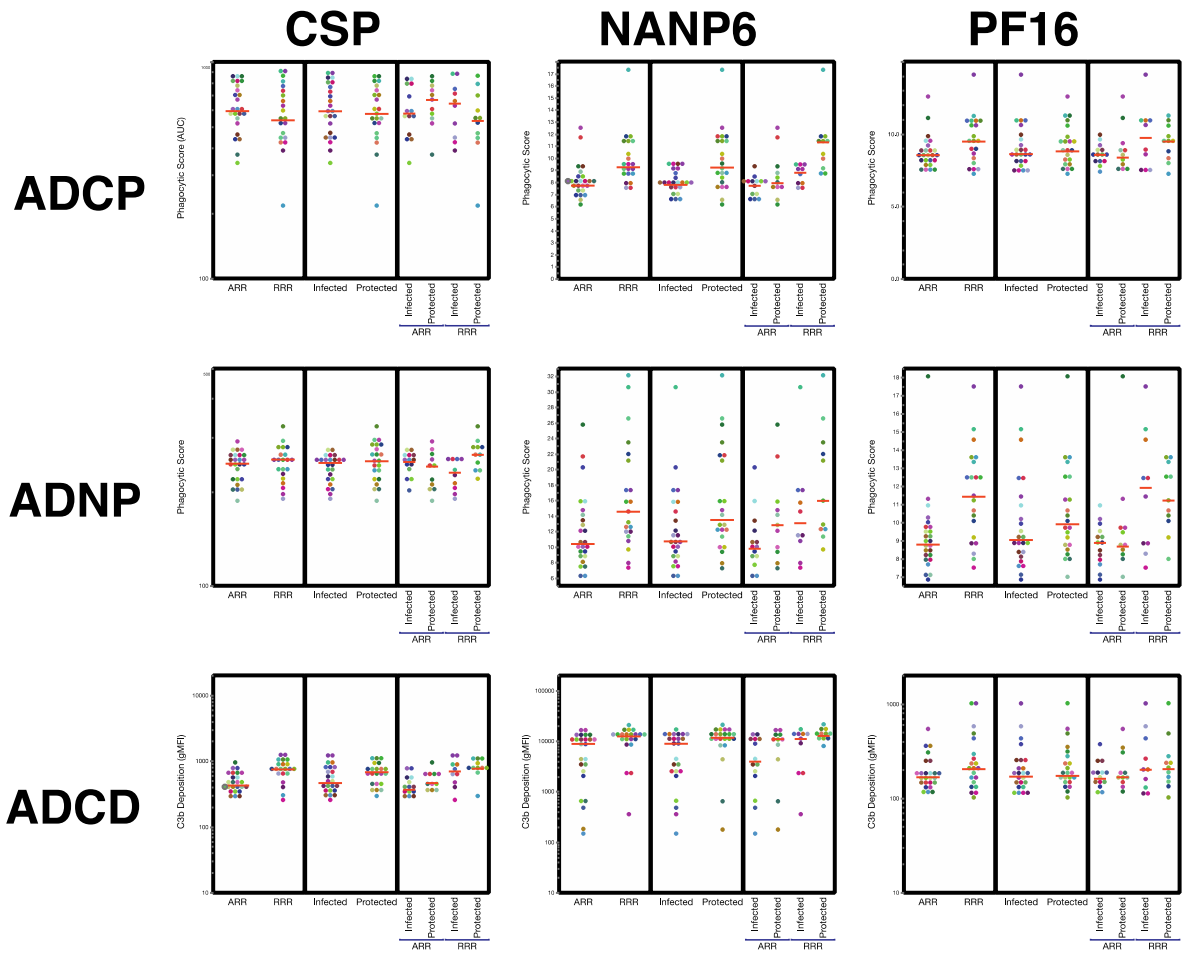

Fig. S1A. Univariate humoral immune response comparisons across MAL068 vaccinees.
The individual antigen-specific features were compared across study arm (i.e., RRR versus ARR), protection status (i.e., protected versus infected), and arm-specific protection (i.e., ARR protected versus ARR infected and RRR protected versus RRR infected).
(A) CSP-, NANP6-, and Pf16-specific functional activity (ADCP, ADNP, and ADCD).
(B) CSP-, NANP6-, and Pf16-specific NK cell activation.
(C) CSP-specific dendritic cell–mediated phagocytosis and dendritic cell activation.
(D) CSP-, NANP6-, and Pf16-specific antibody isotype concentrations.
(E) CSP-, NANP6-, and Pf16-specific IgG subclass concentrations.
(F) CSP-, NANP6-, and Pf16-specific antibody binding to FCGR2A/B.
(G) CSP-, NANP6-, and Pf16-specific antibody binding to FCGR3A/B.
(H) CSP-, NANP6-, and Pf16-specific antibody binding to C1q.
(I-M) NANP-6 and Pf16-specific antibody glycosylation.
(N) Table of unadjusted and adjusted p values. Data were analyzed using a Mann-Whitney U test, and significance was determined following Holm-Šídák correction for multiple comparisons. Values in red are significant following correction for multiple comparisons.

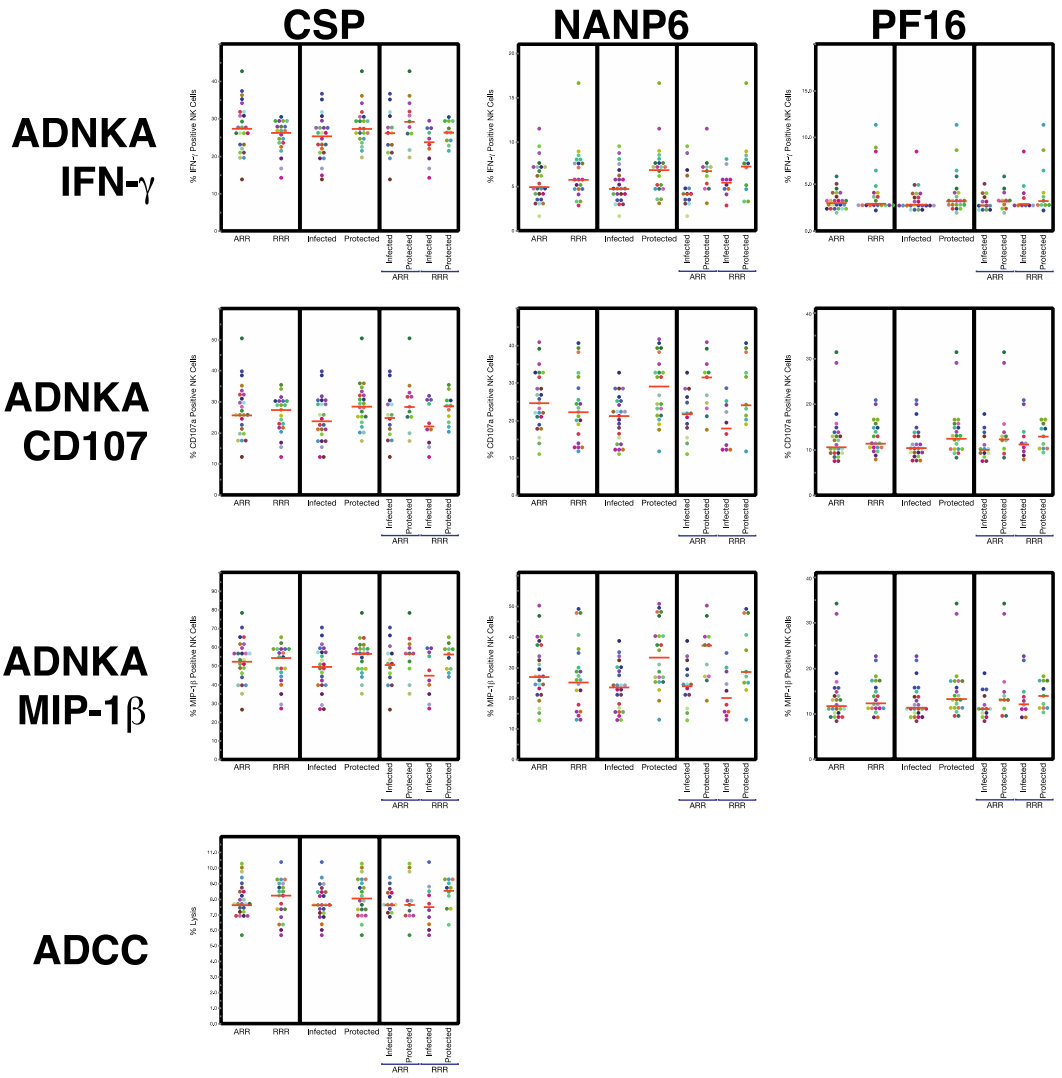

Fig. S1B. Univariate humoral immune response comparisons across MAL068 vaccinees.
The individual antigen-specific features were compared across study arm (i.e., RRR versus ARR), protection status (i.e., protected versus infected), and arm-specific protection (i.e., ARR protected versus ARR infected and RRR protected versus RRR infected).
(A) CSP-, NANP6-, and Pf16-specific functional activity (ADCP, ADNP, and ADCD).
(B) CSP-, NANP6-, and Pf16-specific NK cell activation.
(C) CSP-specific dendritic cell–mediated phagocytosis and dendritic cell activation.
(D) CSP-, NANP6-, and Pf16-specific antibody isotype concentrations.
(E) CSP-, NANP6-, and Pf16-specific IgG subclass concentrations.
(F) CSP-, NANP6-, and Pf16-specific antibody binding to FCGR2A/B.
(G) CSP-, NANP6-, and Pf16-specific antibody binding to FCGR3A/B.
(H) CSP-, NANP6-, and Pf16-specific antibody binding to C1q.
(I-M) NANP-6 and Pf16-specific antibody glycosylation.
(N) Table of unadjusted and adjusted p values. Data were analyzed using a Mann-Whitney U test, and significance was determined following Holm-Šídák correction for multiple comparisons. Values in red are significant following correction for multiple comparisons.

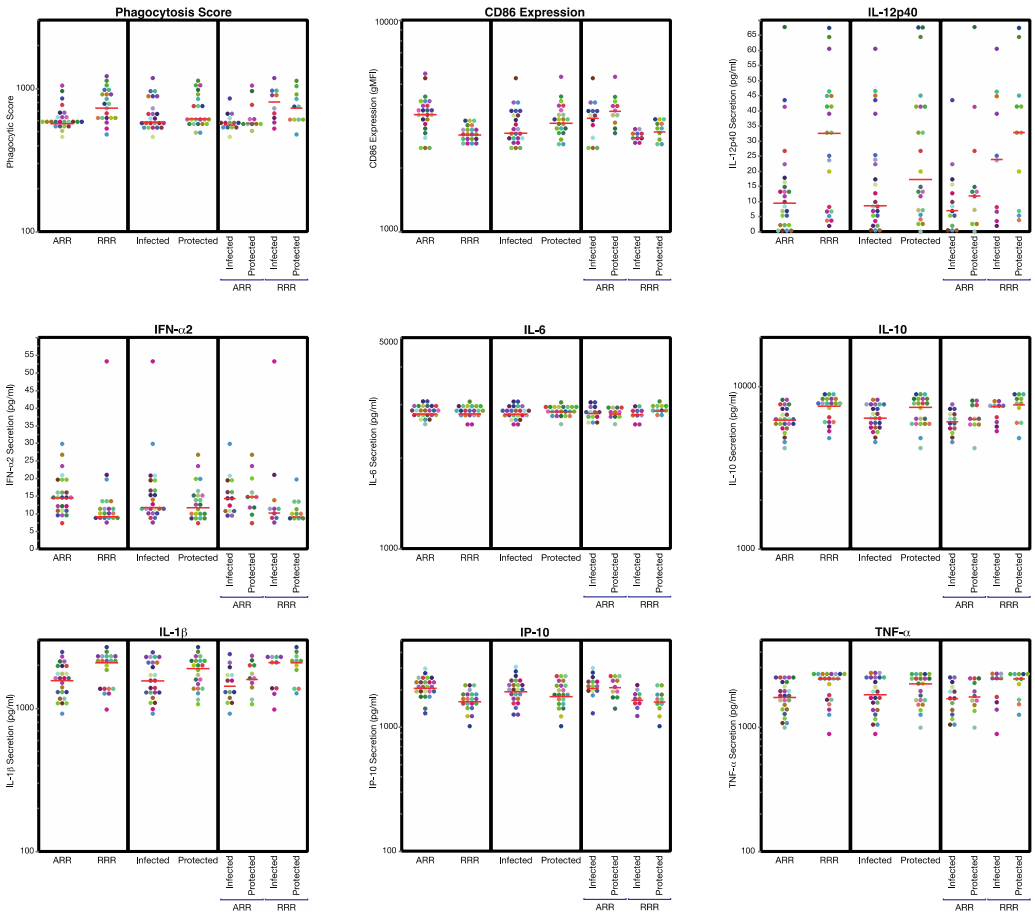

Fig. S1C. Univariate humoral immune response comparisons across MAL068 vaccinees.
The individual antigen-specific features were compared across study arm (i.e., RRR versus ARR), protection status (i.e., protected versus infected), and arm-specific protection (i.e., ARR protected versus ARR infected and RRR protected versus RRR infected).
(A) CSP-, NANP6-, and Pf16-specific functional activity (ADCP, ADNP, and ADCD).
(B) CSP-, NANP6-, and Pf16-specific NK cell activation.
(C) CSP-specific dendritic cell–mediated phagocytosis and dendritic cell activation.
(D) CSP-, NANP6-, and Pf16-specific antibody isotype concentrations.
(E) CSP-, NANP6-, and Pf16-specific IgG subclass concentrations.
(F) CSP-, NANP6-, and Pf16-specific antibody binding to FCGR2A/B.
(G) CSP-, NANP6-, and Pf16-specific antibody binding to FCGR3A/B.
(H) CSP-, NANP6-, and Pf16-specific antibody binding to C1q.
(I-M) NANP-6 and Pf16-specific antibody glycosylation.
(N) Table of unadjusted and adjusted p values. Data were analyzed using a Mann-Whitney U test, and significance was determined following Holm-Šídák correction for multiple comparisons. Values in red are significant following correction for multiple comparisons.

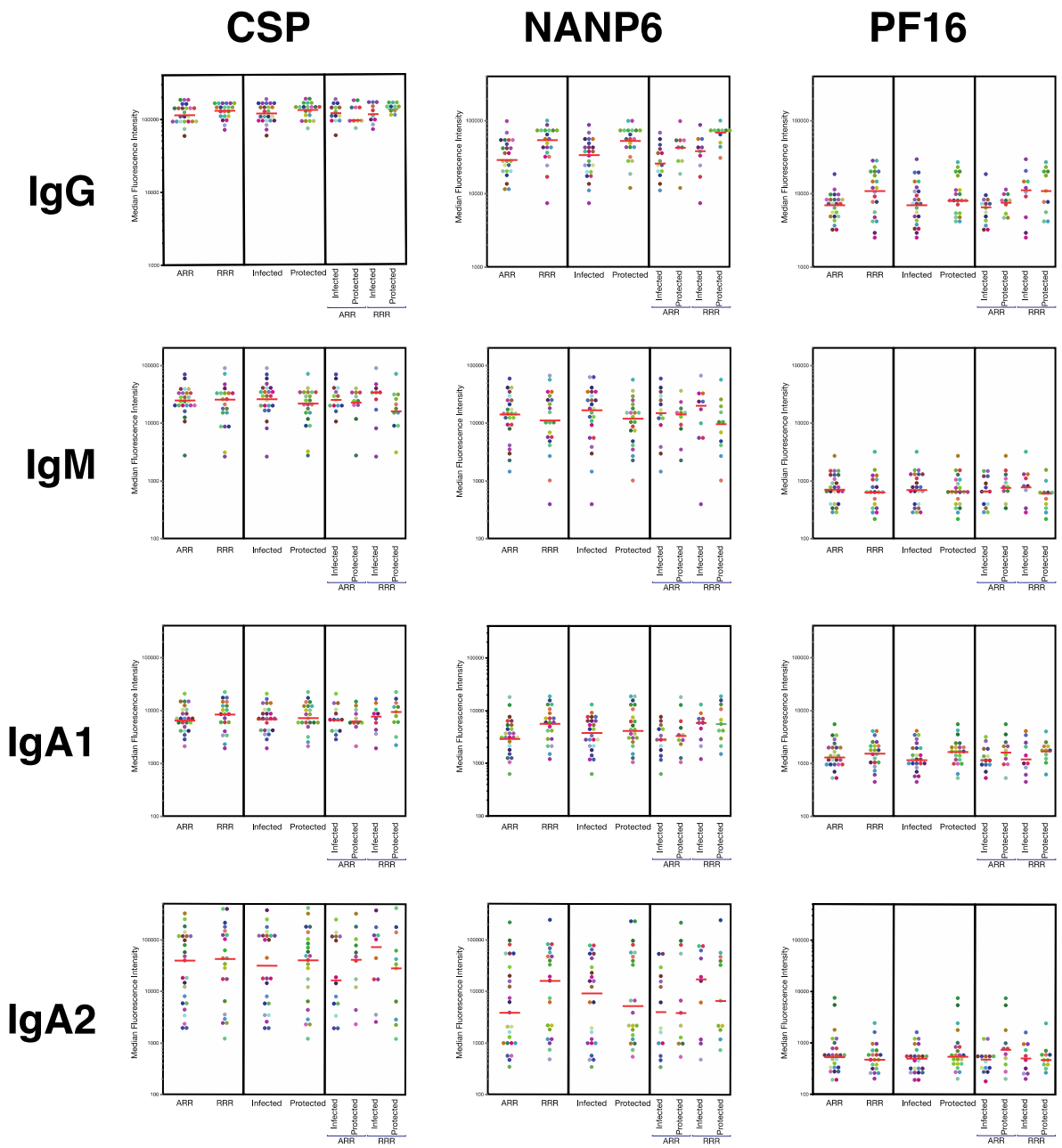

Fig. S1D. Univariate humoral immune response comparisons across MAL068 vaccinees.
The individual antigen-specific features were compared across study arm (i.e., RRR versus ARR), protection status (i.e., protected versus infected), and arm-specific protection (i.e., ARR protected versus ARR infected and RRR protected versus RRR infected).
(A) CSP-, NANP6-, and Pf16-specific functional activity (ADCP, ADNP, and ADCD).
(B) CSP-, NANP6-, and Pf16-specific NK cell activation.
(C) CSP-specific dendritic cell–mediated phagocytosis and dendritic cell activation.
(D) CSP-, NANP6-, and Pf16-specific antibody isotype concentrations.
(E) CSP-, NANP6-, and Pf16-specific IgG subclass concentrations.
(F) CSP-, NANP6-, and Pf16-specific antibody binding to FCGR2A/B.
(G) CSP-, NANP6-, and Pf16-specific antibody binding to FCGR3A/B.
(H) CSP-, NANP6-, and Pf16-specific antibody binding to C1q.
(I-M) NANP-6 and Pf16-specific antibody glycosylation.
(N) Table of unadjusted and adjusted p values. Data were analyzed using a Mann-Whitney U test, and significance was determined following Holm-Šídák correction for multiple comparisons. Values in red are significant following correction for multiple comparisons.

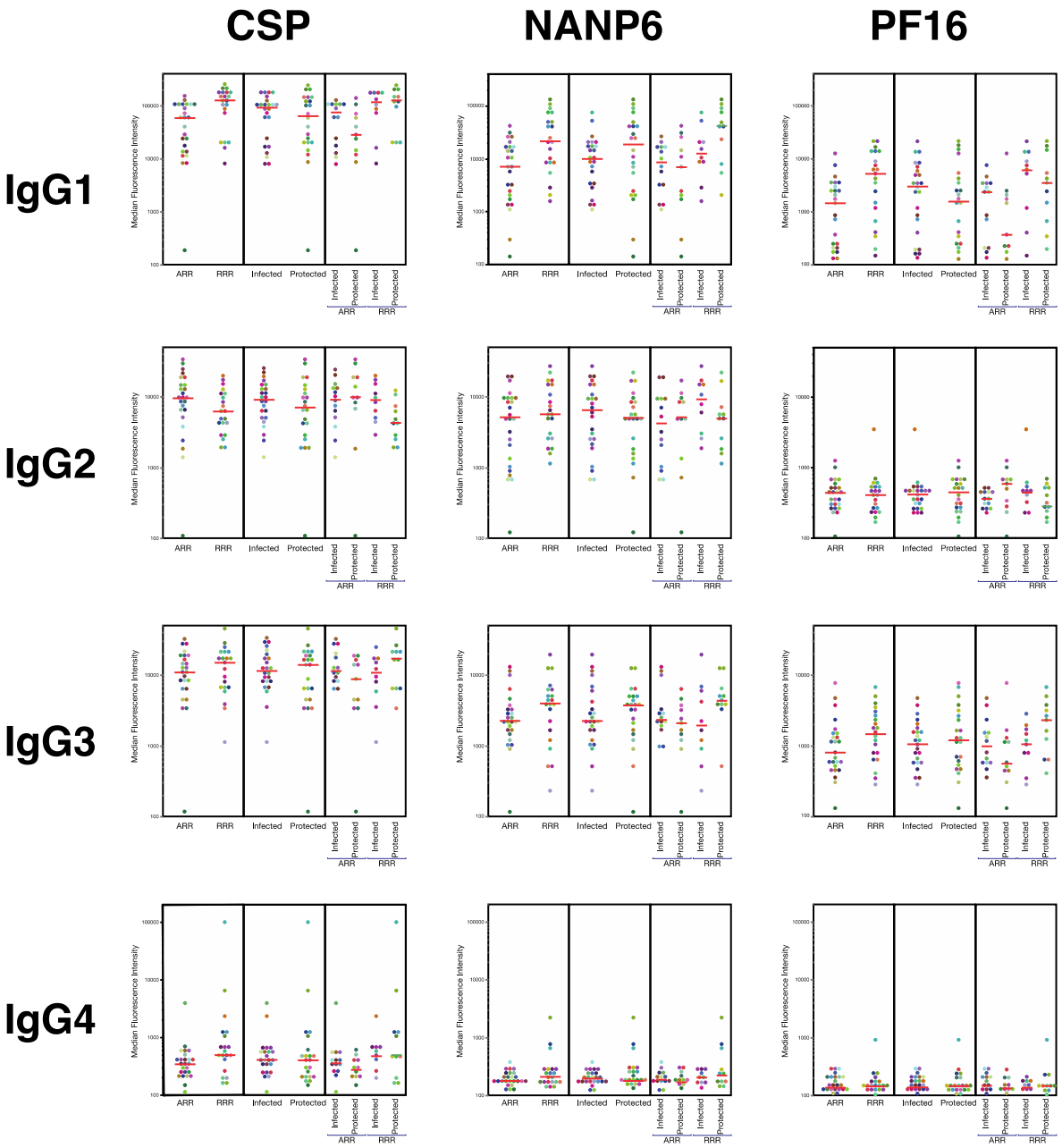

Fig. S1E. Univariate humoral immune response comparisons across MAL068 vaccinees.
The individual antigen-specific features were compared across study arm (i.e., RRR versus ARR), protection status (i.e., protected versus infected), and arm-specific protection (i.e., ARR protected versus ARR infected and RRR protected versus RRR infected).
(A) CSP-, NANP6-, and Pf16-specific functional activity (ADCP, ADNP, and ADCD).
(B) CSP-, NANP6-, and Pf16-specific NK cell activation.
(C) CSP-specific dendritic cell–mediated phagocytosis and dendritic cell activation.
(D) CSP-, NANP6-, and Pf16-specific antibody isotype concentrations.
(E) CSP-, NANP6-, and Pf16-specific IgG subclass concentrations.
(F) CSP-, NANP6-, and Pf16-specific antibody binding to FCGR2A/B.
(G) CSP-, NANP6-, and Pf16-specific antibody binding to FCGR3A/B.
(H) CSP-, NANP6-, and Pf16-specific antibody binding to C1q.
(I-M) NANP-6 and Pf16-specific antibody glycosylation.
(N) Table of unadjusted and adjusted p values. Data were analyzed using a Mann-Whitney U test, and significance was determined following Holm-Šídák correction for multiple comparisons. Values in red are significant following correction for multiple comparisons.

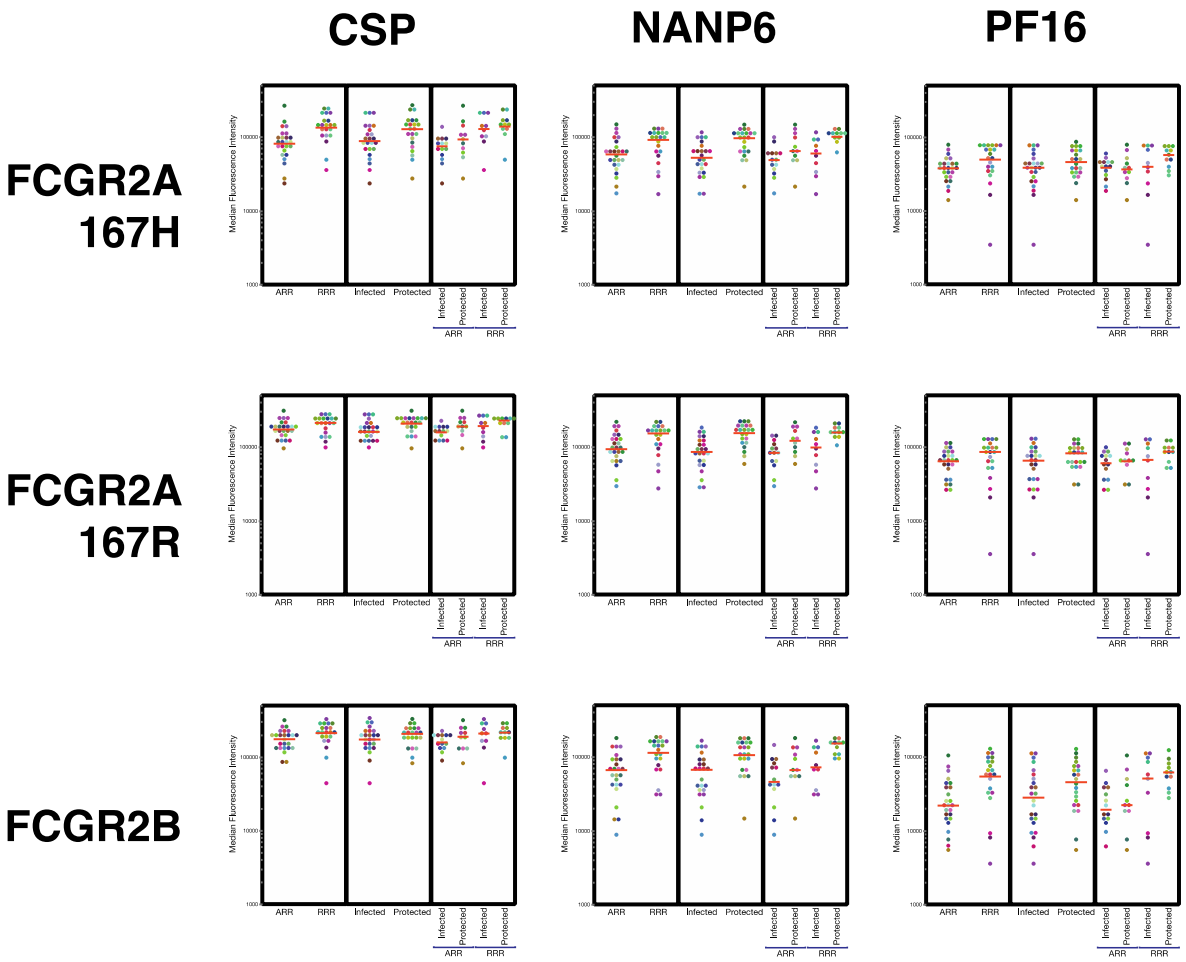

Fig. S1F. Univariate humoral immune response comparisons across MAL068 vaccinees.
The individual antigen-specific features were compared across study arm (i.e., RRR versus ARR), protection status (i.e., protected versus infected), and arm-specific protection (i.e., ARR protected versus ARR infected and RRR protected versus RRR infected).
(A) CSP-, NANP6-, and Pf16-specific functional activity (ADCP, ADNP, and ADCD).
(B) CSP-, NANP6-, and Pf16-specific NK cell activation.
(C) CSP-specific dendritic cell–mediated phagocytosis and dendritic cell activation.
(D) CSP-, NANP6-, and Pf16-specific antibody isotype concentrations.
(E) CSP-, NANP6-, and Pf16-specific IgG subclass concentrations.
(F) CSP-, NANP6-, and Pf16-specific antibody binding to FCGR2A/B.
(G) CSP-, NANP6-, and Pf16-specific antibody binding to FCGR3A/B.
(H) CSP-, NANP6-, and Pf16-specific antibody binding to C1q.
(I-M) NANP-6 and Pf16-specific antibody glycosylation.
(N) Table of unadjusted and adjusted p values. Data were analyzed using a Mann-Whitney U test, and significance was determined following Holm-Šídák correction for multiple comparisons. Values in red are significant following correction for multiple comparisons.

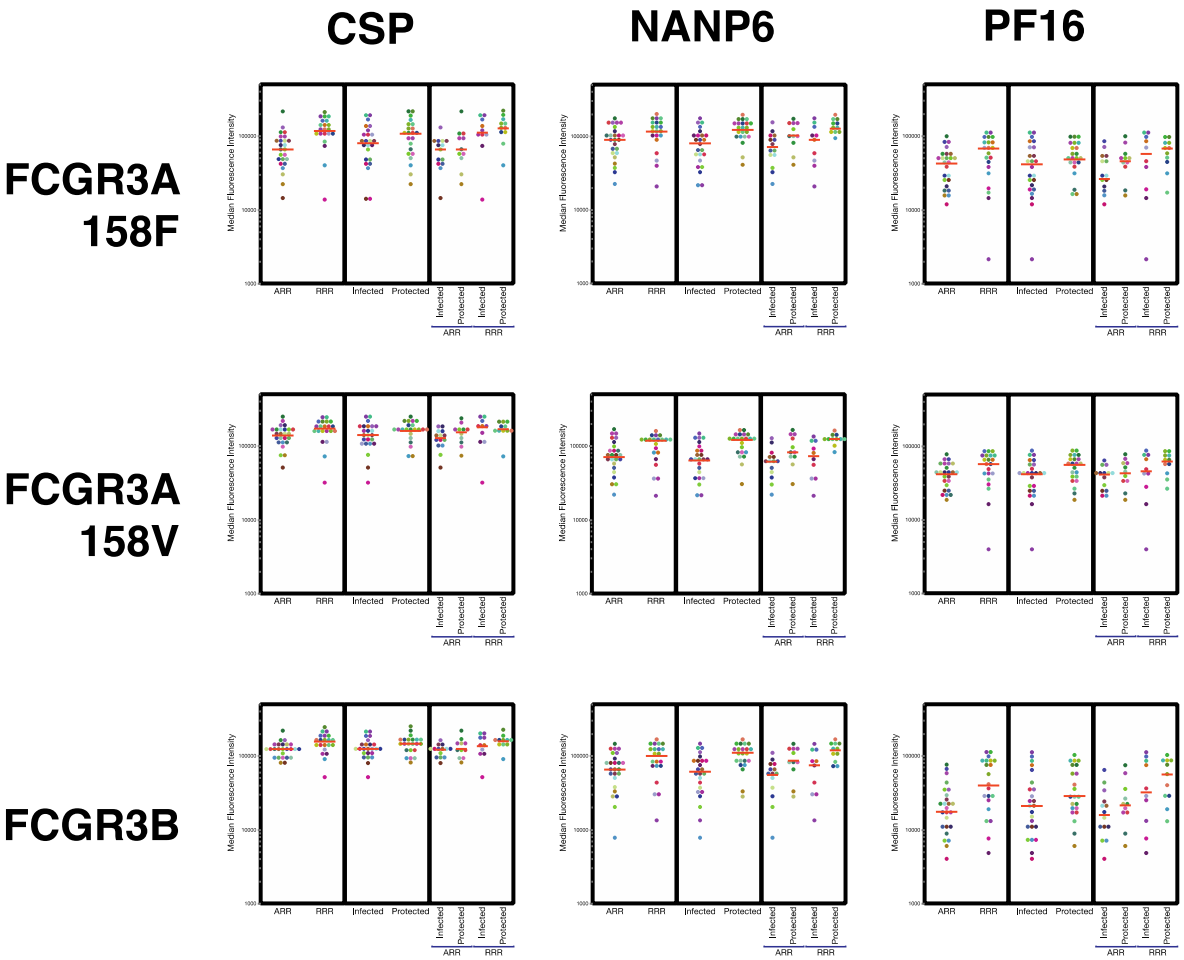

Fig. S1G. Univariate humoral immune response comparisons across MAL068 vaccinees.
The individual antigen-specific features were compared across study arm (i.e., RRR versus ARR), protection status (i.e., protected versus infected), and arm-specific protection (i.e., ARR protected versus ARR infected and RRR protected versus RRR infected).
(A) CSP-, NANP6-, and Pf16-specific functional activity (ADCP, ADNP, and ADCD).
(B) CSP-, NANP6-, and Pf16-specific NK cell activation.
(C) CSP-specific dendritic cell–mediated phagocytosis and dendritic cell activation.
(D) CSP-, NANP6-, and Pf16-specific antibody isotype concentrations.
(E) CSP-, NANP6-, and Pf16-specific IgG subclass concentrations.
(F) CSP-, NANP6-, and Pf16-specific antibody binding to FCGR2A/B.
(G) CSP-, NANP6-, and Pf16-specific antibody binding to FCGR3A/B.
(H) CSP-, NANP6-, and Pf16-specific antibody binding to C1q.
(I-M) NANP-6 and Pf16-specific antibody glycosylation.
(N) Table of unadjusted and adjusted p values. Data were analyzed using a Mann-Whitney U test, and significance was determined following Holm-Šídák correction for multiple comparisons. Values in red are significant following correction for multiple comparisons.

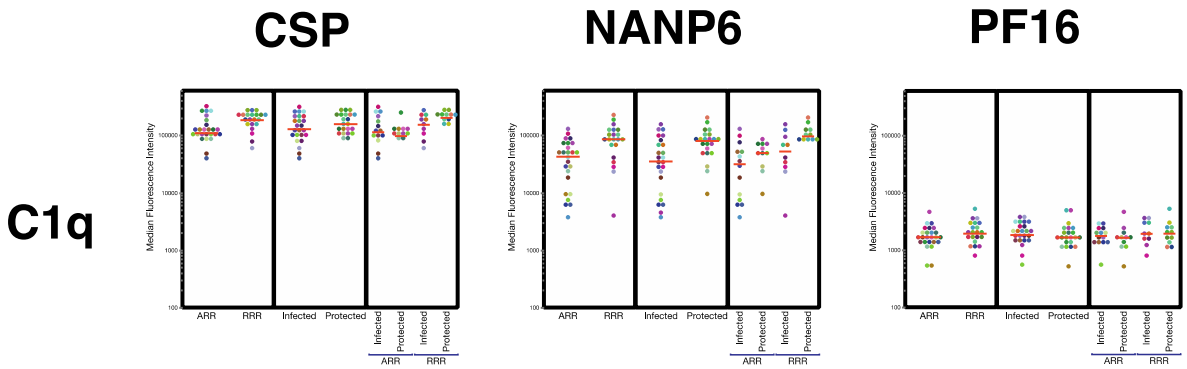

Fig. S1H. Univariate humoral immune response comparisons across MAL068 vaccinees.
The individual antigen-specific features were compared across study arm (i.e., RRR versus ARR), protection status (i.e., protected versus infected), and arm-specific protection (i.e., ARR protected versus ARR infected and RRR protected versus RRR infected).
(A) CSP-, NANP6-, and Pf16-specific functional activity (ADCP, ADNP, and ADCD).
(B) CSP-, NANP6-, and Pf16-specific NK cell activation.
(C) CSP-specific dendritic cell–mediated phagocytosis and dendritic cell activation.
(D) CSP-, NANP6-, and Pf16-specific antibody isotype concentrations.
(E) CSP-, NANP6-, and Pf16-specific IgG subclass concentrations.
(F) CSP-, NANP6-, and Pf16-specific antibody binding to FCGR2A/B.
(G) CSP-, NANP6-, and Pf16-specific antibody binding to FCGR3A/B.
(H) CSP-, NANP6-, and Pf16-specific antibody binding to C1q.
(I-M) NANP-6 and Pf16-specific antibody glycosylation.
(N) Table of unadjusted and adjusted p values. Data were analyzed using a Mann-Whitney U test, and significance was determined following Holm-Šídák correction for multiple comparisons. Values in red are significant following correction for multiple comparisons.

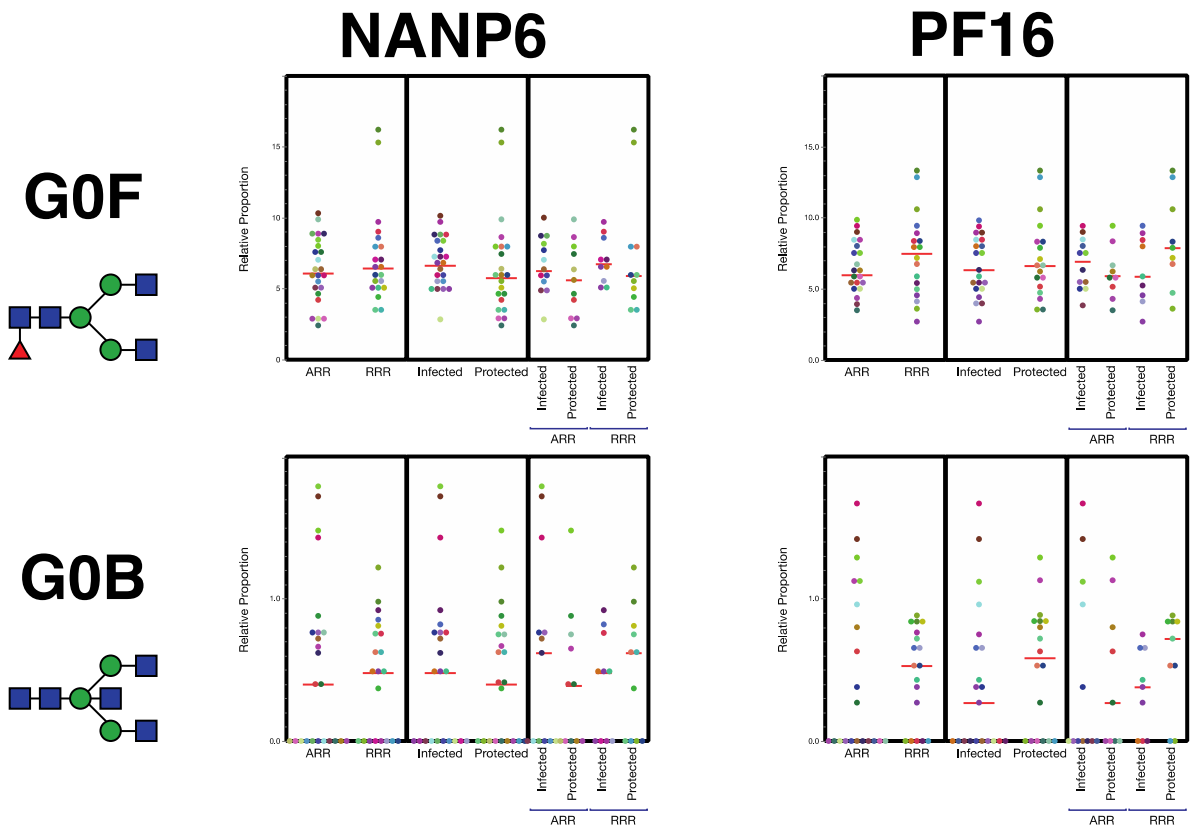

Fig. S1I. Univariate humoral immune response comparisons across MAL068 vaccinees.
The individual antigen-specific features were compared across study arm (i.e., RRR versus ARR), protection status (i.e., protected versus infected), and arm-specific protection (i.e., ARR protected versus ARR infected and RRR protected versus RRR infected).
(A) CSP-, NANP6-, and Pf16-specific functional activity (ADCP, ADNP, and ADCD).
(B) CSP-, NANP6-, and Pf16-specific NK cell activation.
(C) CSP-specific dendritic cell–mediated phagocytosis and dendritic cell activation.
(D) CSP-, NANP6-, and Pf16-specific antibody isotype concentrations.
(E) CSP-, NANP6-, and Pf16-specific IgG subclass concentrations.
(F) CSP-, NANP6-, and Pf16-specific antibody binding to FCGR2A/B.
(G) CSP-, NANP6-, and Pf16-specific antibody binding to FCGR3A/B.
(H) CSP-, NANP6-, and Pf16-specific antibody binding to C1q.
(I-M) NANP-6 and Pf16-specific antibody glycosylation.
(N) Table of unadjusted and adjusted p values. Data were analyzed using a Mann-Whitney U test, and significance was determined following Holm-Šídák correction for multiple comparisons. Values in red are significant following correction for multiple comparisons.

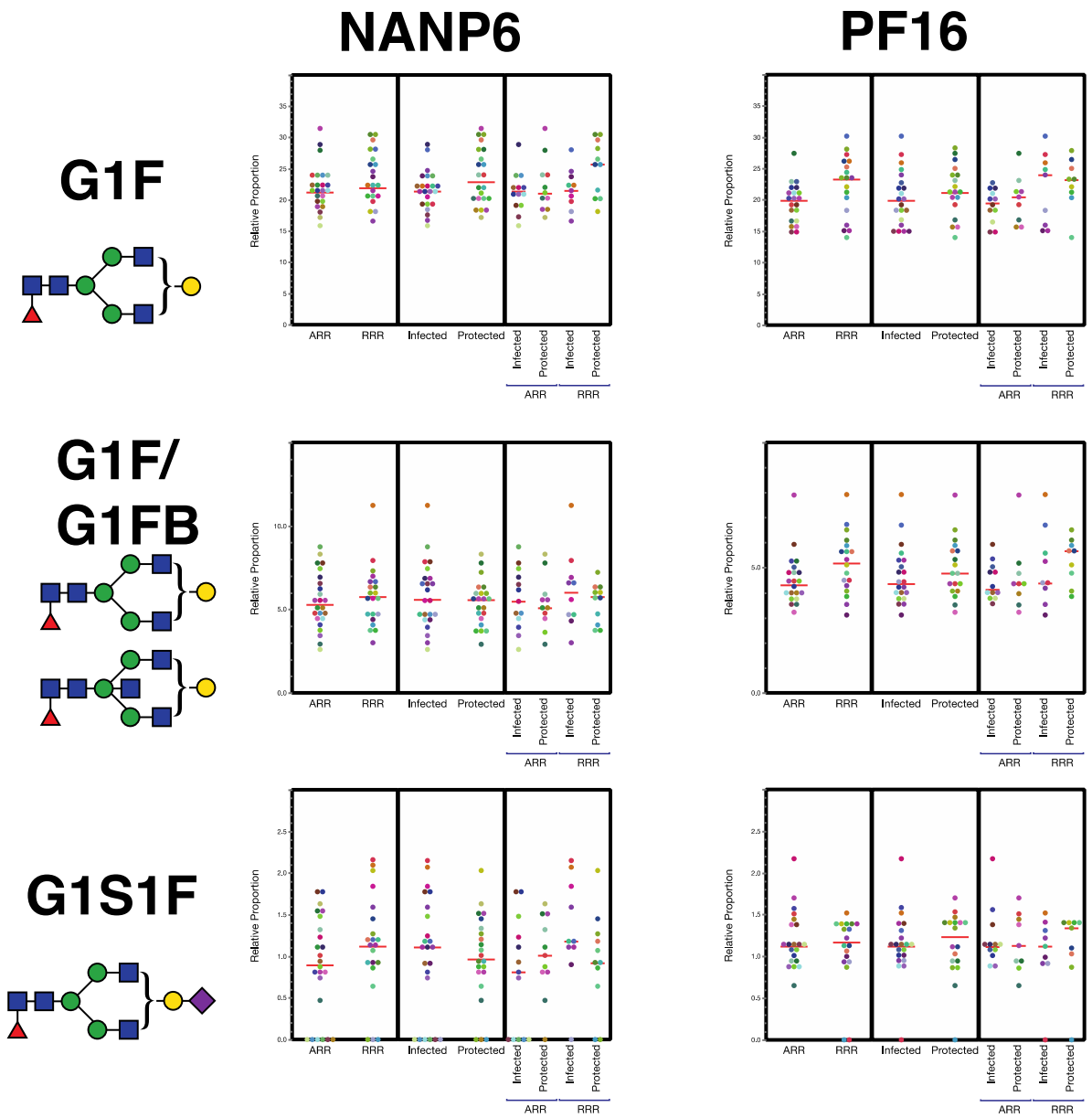

Fig. S1J. Univariate humoral immune response comparisons across MAL068 vaccinees.
The individual antigen-specific features were compared across study arm (i.e., RRR versus ARR), protection status (i.e., protected versus infected), and arm-specific protection (i.e., ARR protected versus ARR infected and RRR protected versus RRR infected).
(A) CSP-, NANP6-, and Pf16-specific functional activity (ADCP, ADNP, and ADCD).
(B) CSP-, NANP6-, and Pf16-specific NK cell activation.
(C) CSP-specific dendritic cell–mediated phagocytosis and dendritic cell activation.
(D) CSP-, NANP6-, and Pf16-specific antibody isotype concentrations.
(E) CSP-, NANP6-, and Pf16-specific IgG subclass concentrations.
(F) CSP-, NANP6-, and Pf16-specific antibody binding to FCGR2A/B.
(G) CSP-, NANP6-, and Pf16-specific antibody binding to FCGR3A/B.
(H) CSP-, NANP6-, and Pf16-specific antibody binding to C1q.
(I-M) NANP-6 and Pf16-specific antibody glycosylation.
(N) Table of unadjusted and adjusted p values. Data were analyzed using a Mann-Whitney U test, and significance was determined following Holm-Šídák correction for multiple comparisons. Values in red are significant following correction for multiple comparisons.

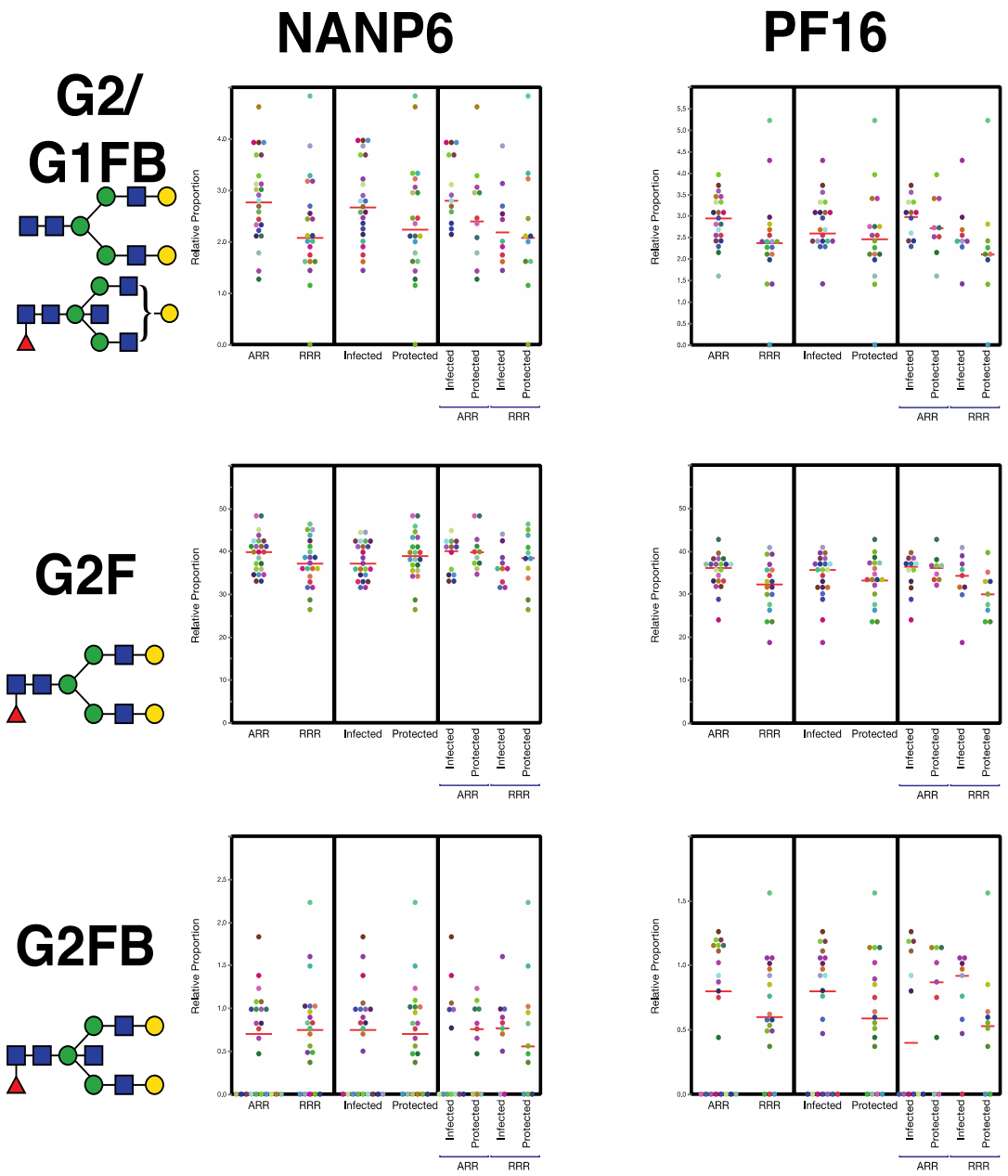

Fig. S1K. Univariate humoral immune response comparisons across MAL068 vaccinees.
The individual antigen-specific features were compared across study arm (i.e., RRR versus ARR), protection status (i.e., protected versus infected), and arm-specific protection (i.e., ARR protected versus ARR infected and RRR protected versus RRR infected).
(A) CSP-, NANP6-, and Pf16-specific functional activity (ADCP, ADNP, and ADCD).
(B) CSP-, NANP6-, and Pf16-specific NK cell activation.
(C) CSP-specific dendritic cell–mediated phagocytosis and dendritic cell activation.
(D) CSP-, NANP6-, and Pf16-specific antibody isotype concentrations.
(E) CSP-, NANP6-, and Pf16-specific IgG subclass concentrations.
(F) CSP-, NANP6-, and Pf16-specific antibody binding to FCGR2A/B.
(G) CSP-, NANP6-, and Pf16-specific antibody binding to FCGR3A/B.
(H) CSP-, NANP6-, and Pf16-specific antibody binding to C1q.
(I-M) NANP-6 and Pf16-specific antibody glycosylation.
(N) Table of unadjusted and adjusted p values. Data were analyzed using a Mann-Whitney U test, and significance was determined following Holm-Šídák correction for multiple comparisons. Values in red are significant following correction for multiple comparisons.

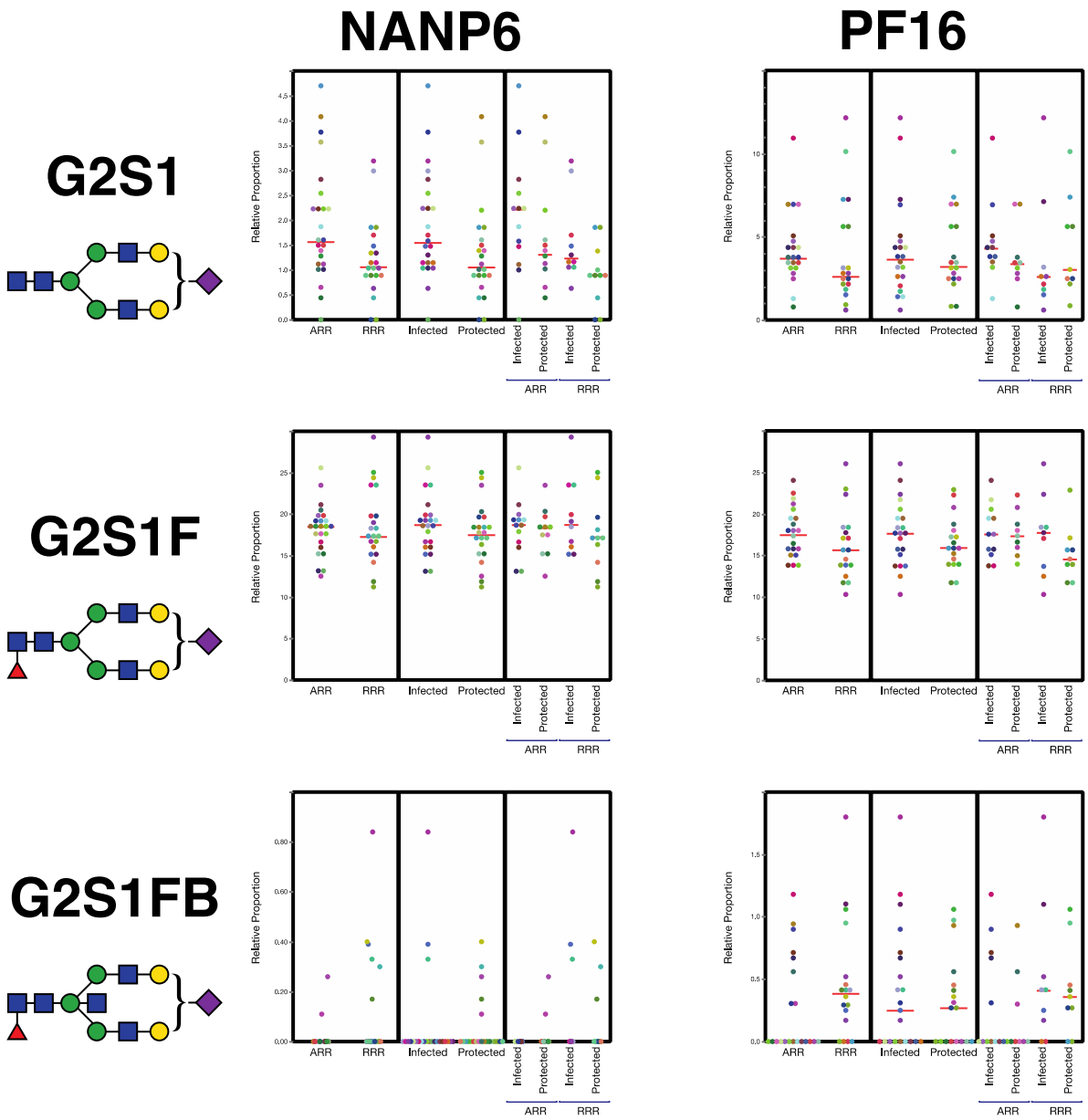

Fig. S1L. Univariate humoral immune response comparisons across MAL068 vaccinees.
The individual antigen-specific features were compared across study arm (i.e., RRR versus ARR), protection status (i.e., protected versus infected), and arm-specific protection (i.e., ARR protected versus ARR infected and RRR protected versus RRR infected).
(A) CSP-, NANP6-, and Pf16-specific functional activity (ADCP, ADNP, and ADCD).
(B) CSP-, NANP6-, and Pf16-specific NK cell activation.
(C) CSP-specific dendritic cell–mediated phagocytosis and dendritic cell activation.
(D) CSP-, NANP6-, and Pf16-specific antibody isotype concentrations.
(E) CSP-, NANP6-, and Pf16-specific IgG subclass concentrations.
(F) CSP-, NANP6-, and Pf16-specific antibody binding to FCGR2A/B.
(G) CSP-, NANP6-, and Pf16-specific antibody binding to FCGR3A/B.
(H) CSP-, NANP6-, and Pf16-specific antibody binding to C1q.
(I-M) NANP-6 and Pf16-specific antibody glycosylation.
(N) Table of unadjusted and adjusted p values. Data were analyzed using a Mann-Whitney U test, and significance was determined following Holm-Šídák correction for multiple comparisons. Values in red are significant following correction for multiple comparisons.

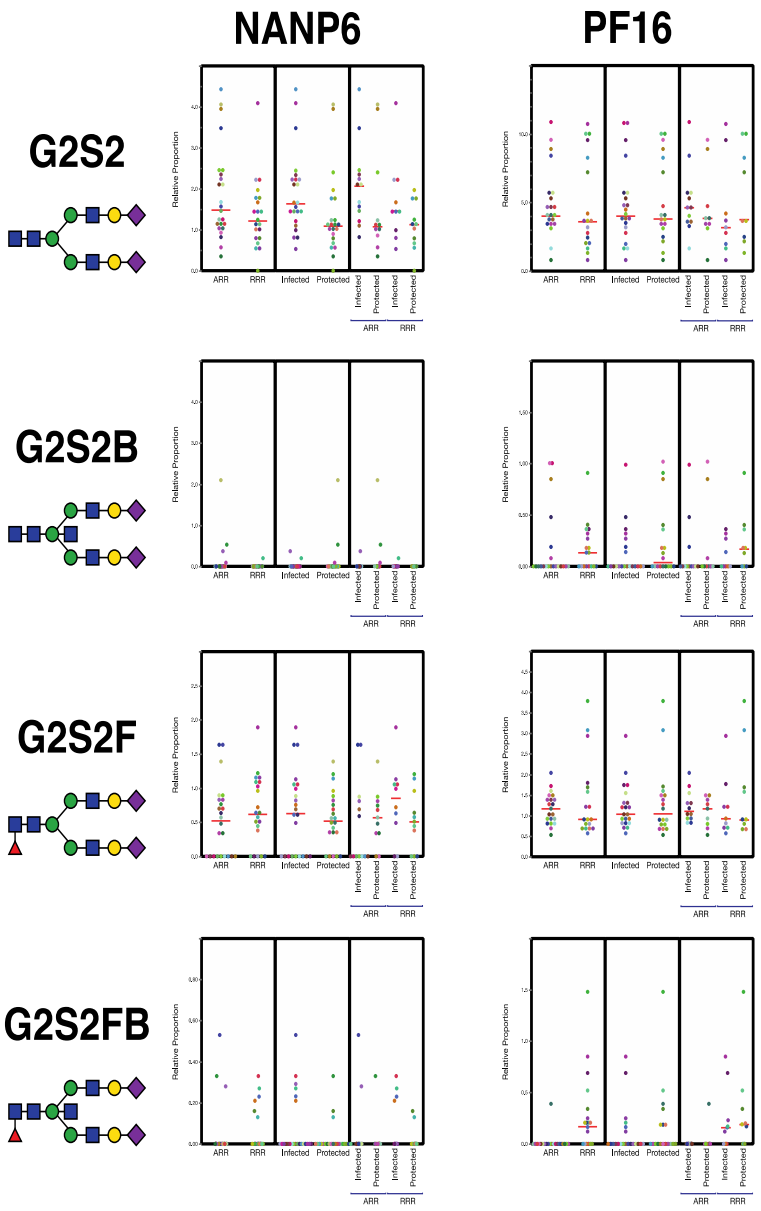

Fig. S1M. Univariate humoral immune response comparisons across MAL068 vaccinees.
The individual antigen-specific features were compared across study arm (i.e., RRR versus ARR), protection status (i.e., protected versus infected), and arm-specific protection (i.e., ARR protected versus ARR infected and RRR protected versus RRR infected).
(A) CSP-, NANP6-, and Pf16-specific functional activity (ADCP, ADNP, and ADCD).
(B) CSP-, NANP6-, and Pf16-specific NK cell activation.
(C) CSP-specific dendritic cell–mediated phagocytosis and dendritic cell activation.
(D) CSP-, NANP6-, and Pf16-specific antibody isotype concentrations.
(E) CSP-, NANP6-, and Pf16-specific IgG subclass concentrations.
(F) CSP-, NANP6-, and Pf16-specific antibody binding to FCGR2A/B.
(G) CSP-, NANP6-, and Pf16-specific antibody binding to FCGR3A/B.
(H) CSP-, NANP6-, and Pf16-specific antibody binding to C1q.
(I-M) NANP-6 and Pf16-specific antibody glycosylation.
(N) Table of unadjusted and adjusted p values. Data were analyzed using a Mann-Whitney U test, and significance was determined following Holm-Šídák correction for multiple comparisons. Values in red are significant following correction for multiple comparisons.

Feature	ARR vs. RRR		Protected vs. Infected					
			Combined		ARR Only		RRR Only	
	Unadjusted	Adjusted	Unadjusted	Adjusted	Unadjusted	Adjusted	Unadjusted	Adjusted
ADNP: CSP	0.5416	1	0.1982	1	0.3668	1	0.0075	0.5464
ADNP: NANP6	0.0231	0.866	0.0481	0.9907	0.1402	1	0.2414	1
ADNP: Pf16	0.0023	0.2075	0.4759	1	0.325	1	0.7747	1
ADCP: CSP-AUC	0.4886	1	0.7322	1	0.542	1	0.3605	1
ADCP: NANP6	0.002	0.1847	0.0038	0.3244	0.1647	1	0.0063	0.4915
ADCP: Pf16	0.0596	0.9827	0.8679	1	0.5917	1	0.6739	1
ADDCP: CSP- Phagocytosis Score	0.0065	0.4653	0.5203	1	0.2051	1	0.6495	1
ADDCP: CSP-CD86 Expression	0.0001	0.011	0.2925	1	0.2726	1	0.065	0.9976
ADDCP-CSP: IFN-a2	0.3263	1	0.3576	1	0.9116	1	0.3419	1
ADDCP-CSP: IL-10	0.0087	0.5602	0.1345	1	0.2692	1	0.4287	1
ADDCP-CSP: IL-12p40	0.0097	0.5961	0.1597	1	0.2905	1	0.4734	1
ADDCP-CSP: IL-1β	0.0232	0.866	0.2287	1	0.3384	1	0.5911	1
ADDCP-CSP: IL-6	0.7555	1	0.1761	1	0.9845	1	0.0379	0.9755
ADDCP-CSP: IP-10	<0.0001	<0.011	0.5398	1	0.7715	1	0.8426	1
ADDCP-CSP: TNF-α	0.0149	0.7331	0.2938	1	0.5327	1	0.5365	1
ADCC: CSP	0.9155	1	0.3424	1	0.9989	1	0.2035	1
ADNKA: CSP-IFNγ	0.0996	0.9987	0.0492	0.9913	0.1643	1	0.0875	0.9997
ADNKA: CSP-CD107a	0.4835	1	0.0387	0.9776	0.2022	1	0.0784	0.9992
ADNKA: CSP-MIP1β	0.4306	1	0.0384	0.9776	0.3197	1	0.0469	0.9891
ADNKA: NANP6-IFNγ	0.279	1	0.0256	0.9233	0.0868	0.9999	0.158	1
ADNKA: NANP6-CD107a	0.4372	1	0.0007	0.0709	0.0107	0.6871	0.0207	0.8739
ADNKA: NANP6-MIP1β	0.6278	1	0.0004	0.0423	0.0093	0.6388	0.0173	0.8284
ADNKA: PF16-IFNγ	0.0876	0.9972	0.2667	1	0.4937	1	0.4269	1
ADNKA: PF16-CD107a	0.9706	1	0.1085	0.9999	0.1091	1	0.8939	1
ADNKA: PF16-MIP1β	0.9508	1	0.104	0.9999	0.1194	1	0.8224	1
ADCD: CSP	0.0002	0.0216	0.1651	1	0.1616	1	0.614	1
ADCD: NANP6	0.0128	0.6823	0.0147	0.7792	0.1136	1	0.1103	1
ADCD: Pf16	0.001	0.1006	0.4318	1	0.1645	1	0.7288	1
FCGR2A (H): CSP	0.0015	0.1458	0.1353	1	0.1601	1	0.6884	1
FCGR2A (R): CSP	0.051	0.9757	0.0339	0.9659	0.0813	0.9998	0.3412	1
FCGR2B: CSP	0.0429	0.9658	0.1843	1	0.1721	1	0.7811	1
FCGR3A (F): CSP	0.0003	0.0319	0.252	1	0.3468	1	0.6974	1
FCGR3A (V): CSP	0.0296	0.9174	0.2633	1	0.2689	1	0.7913	1
FCGR3B: CSP	0.0151	0.7339	0.1018	0.9999	0.2936	1	0.3256	1
C1q: CSP	0.0125	0.6776	0.4644	1	0.3168	1	0.0255	0.9184
FCGR2A (H): NANP6	0.0408	0.9612	0.0003	0.0322	0.0557	0.9973	0.005	0.418
FCGR2A (R): NANP6	0.0302	0.9191	0.0002	0.0218	0.0242	0.9255	0.0069	0.52
FCGR2B: NANP6	0.0033	0.2791	0.0025	0.2292	0.103	1	0.0125	0.7297
FCGR3A (F): NANP6	0.0778	0.9948	0.0004	0.0423	0.03	0.9587	0.0127	0.7319
FCGR3A (V): NANP6	0.0392	0.9582	0.0001	0.011	0.0299	0.9587	0.0035	0.3176
FCGR3B: NANP6	0.0389	0.9582	0.0006	0.0616	0.0237	0.9232	0.0226	0.8936
C1q: R32LR	0.0008	0.0821	0.0189	0.8516	0.4269	1	0.0192	0.8561
FCGR2A (H): Pf16	0.0503	0.9757	0.1994	1	0.5819	1	0.3442	1
FCGR2A (R): Pf16	0.1311	0.9997	0.0652	0.9979	0.2648	1	0.2268	1
FCGR2B: Pf16	0.0018	0.1694	0.2436	1	0.3563	1	0.6187	1
FCGR3A (F): Pf16	0.0382	0.9574	0.2549	1	0.2538	1	0.7403	1
FCGR3A (V): Pf16	0.0505	0.9757	0.116	1	0.3346	1	0.318	1
FCGR3B: Pf16	0.0023	0.2075	0.2765	1	0.3771	1	0.6112	1
C1q: Pf16	0.202	1	0.9809	1	0.9548	1	0.9538	1
IgG: CSP	0.3062	1	0.703	1	0.5949	1	0.1257	1
IgG1: CSP	0.0016	0.1534	0.9567	1	0.294	1	0.7814	1
IgG2: CSP	0.0479	0.9735	0.8357	1	0.3293	1	0.0433	0.9851
IgG3: CSP	0.5234	1	0.981	1	0.0916	0.9999	0.1651	1
IgG4: CSP	0.2911	1	0.3172	1	0.2777	1	0.3127	1
IgGA1: CSP	0.39	1	0.6481	1	0.6707	1	0.377	1
IgGA2: CSP	0.5104	1	0.8787	1	0.6492	1	0.8088	1
IgM: CSP	0.985	1	0.1386	1	0.3114	1	0.2946	1
IgG: NANP6	0.0102	0.6106	0.0181	0.842	0.4018	1	0.0166	0.8187
IgG1: NANP6	0.0055	0.4143	0.0646	0.9979	0.6926	1	0.0683	0.9982
IgG2: NANP6	0.2928	1	0.444	1	0.9741	1	0.2639	1
IgG3: NANP6	0.2118	1	0.8889	1	0.2027	1	0.5759	1
IgG4: NANP6	0.16	0.9999	0.2229	1	0.4546	1	0.1919	1
IgGA1: NANP6	0.0454	0.9707	0.1021	0.9999	0.2223	1	0.3828	1
IgGA2: NANP6	0.5824	1	0.2159	1	0.2145	1	0.7215	1
IgM: NANP6	0.9069	1	0.168	1	0.3135	1	0.3501	1
IgG: Pf16	0.0049	0.3821	0.5882	1	0.913	1	0.7599	1
IgG1: Pf16	0.0067	0.472	0.857	1	0.7602	1	0.7273	1
IgG2: Pf16	0.6408	1	0.8106	1	0.0733	0.9996	0.3118	1
IgG3: Pf16	0.3188	1	0.2249	1	0.9412	1	0.0597	0.9965
IgG4: Pf16	0.56	1	0.496	1	0.4042	1	0.307	1
IgGA1: Pf16	0.8336	1	0.2712	1	0.2324	1	0.8893	1
IgGA2: Pf16	0.2546	1	0.1226	1	0.1264	1	0.9296	1
IgM: Pf16	0.6461	1	0.8675	1	0.3014	1	0.2742	1
G2S2FB: NANP6	0.6645	1	0.1497	1	0.5538	1	0.1249	1
G2S2F: NANP6	0.3846	1	0.6156	1	0.7041	1	0.2273	1
G2S2B: NANP6	0.1988	1	0.3278	1	0.2833	1	0.3434	1
G2S2: NANP6	0.1172	0.9995	0.0713	0.9986	0.3401	1	0.1272	1
G2S1FB: NANP6	0.0539	0.9777	0.8135	1	0.2036	1	0.4543	1
G2S1F: NANP6	0.7258	1	0.2788	1	0.744	1	0.2725	1
G2S1B: NANP6	0.7871	1	0.1764	1	0.337	1	0.3434	1
G2S1: NANP6	0.0241	0.8712	0.0703	0.9986	0.3902	1	0.0641	0.9976
G2FB: NANP6	0.4261	1	0.7389	1	0.6855	1	0.9942	1
G2F: NANP6	0.1541	0.9999	0.4013	1	0.4066	1	0.6069	1
G2: NANP6	0.0556	0.9784	0.2303	1	0.1726	1	0.8003	1
G1S1F: NANP6	0.1893	1	0.8847	1	0.3239	1	0.1817	1
G1FB: NANP6	0.6042	1	0.3823	1	0.7466	1	0.3704	1
G1F: NANP6	0.168	1	0.0599	0.9968	0.5435	1	0.0512	0.9925
G1B: NANP6	0.656	1	0.7095	1	0.4583	1	0.6102	1
G1: NANP6	0.3277	1	0.3287	1	0.3409	1		
G0F: NANP6	0.2498	1	0.77	1	0.3409	1	0.7994	1
G2S2FB: Pf16	0.0103	0.6106	0.4446	1	0.3466	1	0.6924	1
G2S2F: Pf16	0.3416	1	0.6741	1	0.3483	1	0.4469	1
G2S2B: Pf16	0.9269	1	0.3262	1	0.6371	1	0.3014	1
G2S2: Pf16	0.9644	1	0.7955	1	0.6703	1	0.4981	1
G2S1FB: Pf16	0.1574	0.9999	0.5064	1	0.5017	1	0.6713	1
G2S1F: Pf16	0.2294	1	0.2853	1	0.8297	1	0.3015	1
G2S1B: Pf16	0.0471	0.9732	0.4298	1	0.3466	1	0.6648	1
G2S1: Pf16	0.8305	1	0.8159	1	0.3445	1	0.6834	1
G2FB: Pf16	0.8036	1	0.9593	1	0.4322	1	0.3263	1
G2F: Pf16	0.0483	0.9735	0.5591	1	0.4906	1	0.3032	1
G2: Pf16	0.1214	0.9996	0.34	1	0.5281	1	0.5312	1
G1S1F: Pf16	0.3225	1	0.9249	1	0.7726	1	0.8318	1
G1S1: Pf16	0.3313	1	0.3293	1			0.3466	1
G1FB: Pf16	0.1007	0.9987	0.4717	1	0.7014	1	0.6639	1
G1F: Pf16	0.0536	0.9777	0.4419	1	0.5598	1	0.7301	1
G1B: Pf16	0.9908	1	0.5042	1	0.9854	1	0.1621	1
G1: Pf16	0.1639	0.9999	0.8226	1	0.7597	1		
G0FB: Pf16	0.6157	1	0.5291	1	0.3466	1	0.3466	1
G0F: Pf16	0.2837	1	0.4294	1	0.4367	1	0.171	1
G0B: Pf16	0.3313	1	0.3293	1			0.3466	1
Man3: Pf16	0.553	1	0.3295	1	0.3026	1	0.6985	1

Fig. S1N. Univariate humoral immune response comparisons across MAL068 vaccinees.
The individual antigen-specific features were compared across study arm (i.e., RRR versus ARR), protection status (i.e., protected versus infected), and arm-specific protection (i.e., ARR protected versus ARR infected and RRR protected versus RRR infected).
(A) CSP-, NANP6-, and Pf16-specific functional activity (ADCP, ADNP, and ADCD).
(B) CSP-, NANP6-, and Pf16-specific NK cell activation.
(C) CSP-specific dendritic cell–mediated phagocytosis and dendritic cell activation.
(D) CSP-, NANP6-, and Pf16-specific antibody isotype concentrations.
(E) CSP-, NANP6-, and Pf16-specific IgG subclass concentrations.
(F) CSP-, NANP6-, and Pf16-specific antibody binding to FCGR2A/B.
(G) CSP-, NANP6-, and Pf16-specific antibody binding to FCGR3A/B.
(H) CSP-, NANP6-, and Pf16-specific antibody binding to C1q.
(I-M) NANP-6 and Pf16-specific antibody glycosylation.
(N) Table of unadjusted and adjusted p values. Data were analyzed using a Mann-Whitney U test, and significance was determined following Holm-Šídák correction for multiple comparisons. Values in red are significant following correction for multiple comparisons.

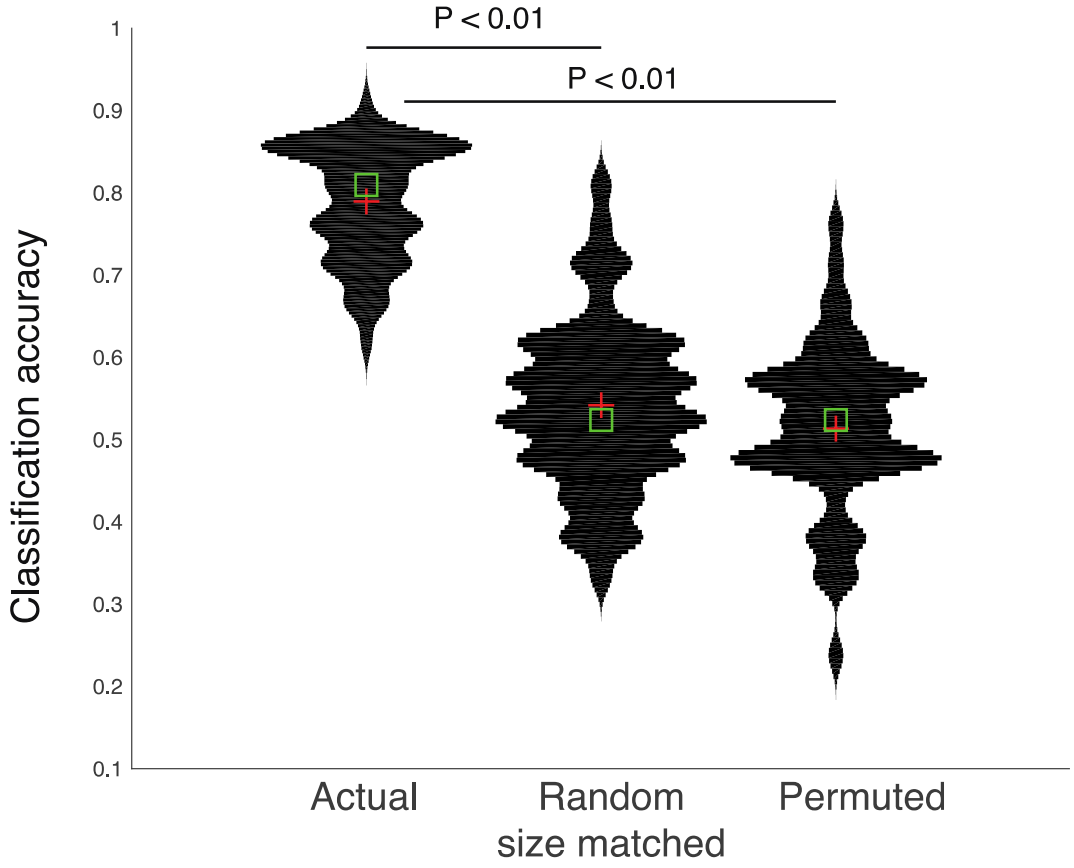

Fig. S2. Model performance in RRR vaccinees.
The violin plot shows the distribution of classification accuracies of the real model across cross-validation replicates, as measured in a tenfold cross-validation framework, compared to the classification accuracies of a model on permuted data or randomly selected data in a matched tenfold cross-validation framework for the RRR arm. The red cross and green square indicate the mean and median of the distribution, respectively. Exact P values were computed using a permutation test.

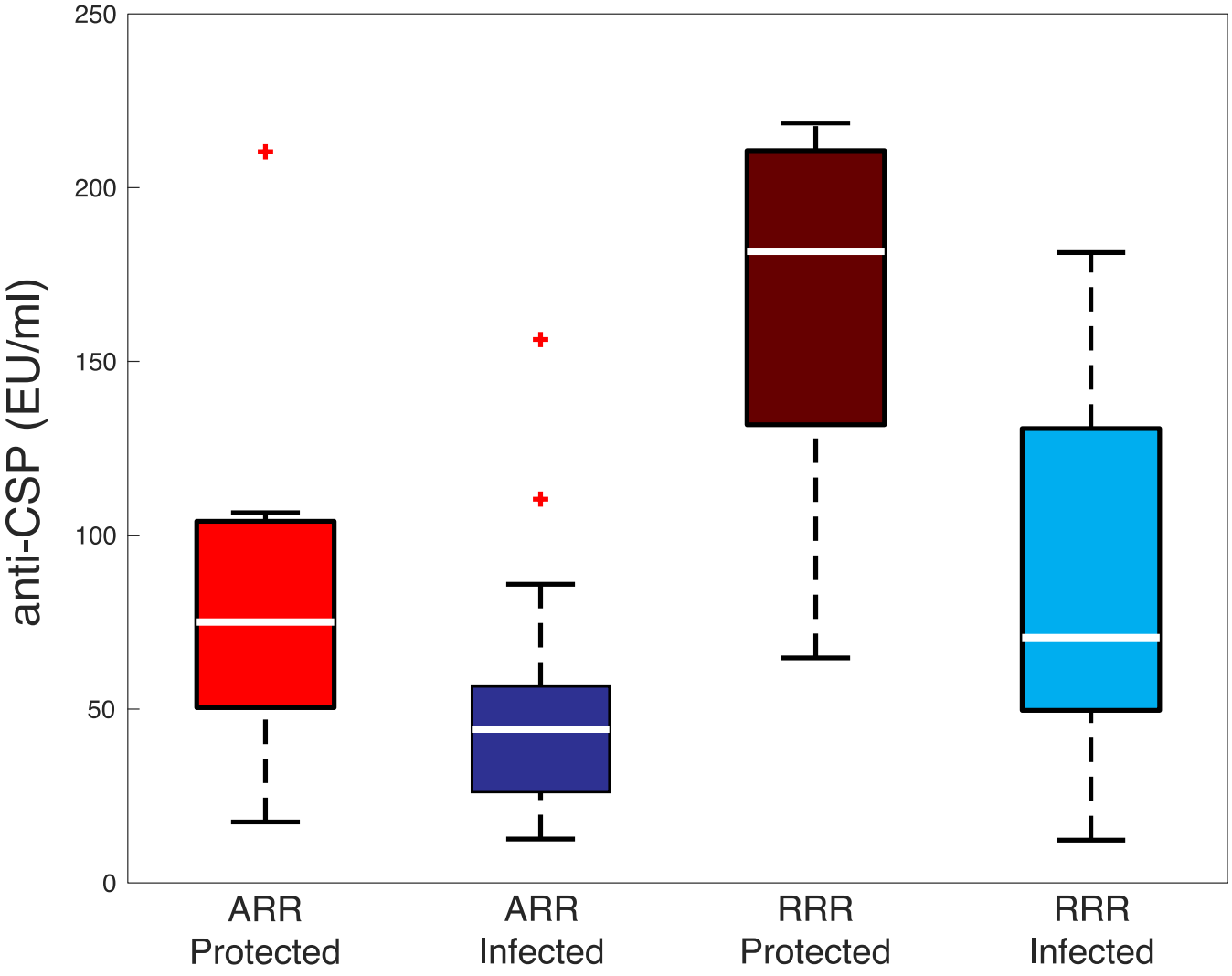

Fig. S3. Different concentrations of CSP-specific antibodies track with protection within arms.
The whisker box plot depicts the concentrations of CSP-specific IgG antibodies across protected and non-protected vaccinees in the ARR and RRR arms of the study. The ends of the box represent the 25th and 75th quantiles; the horizontal line within the box represents the median sample value, and the whiskers represent the upper and lower data point values. Outliers are indicated by crosses.

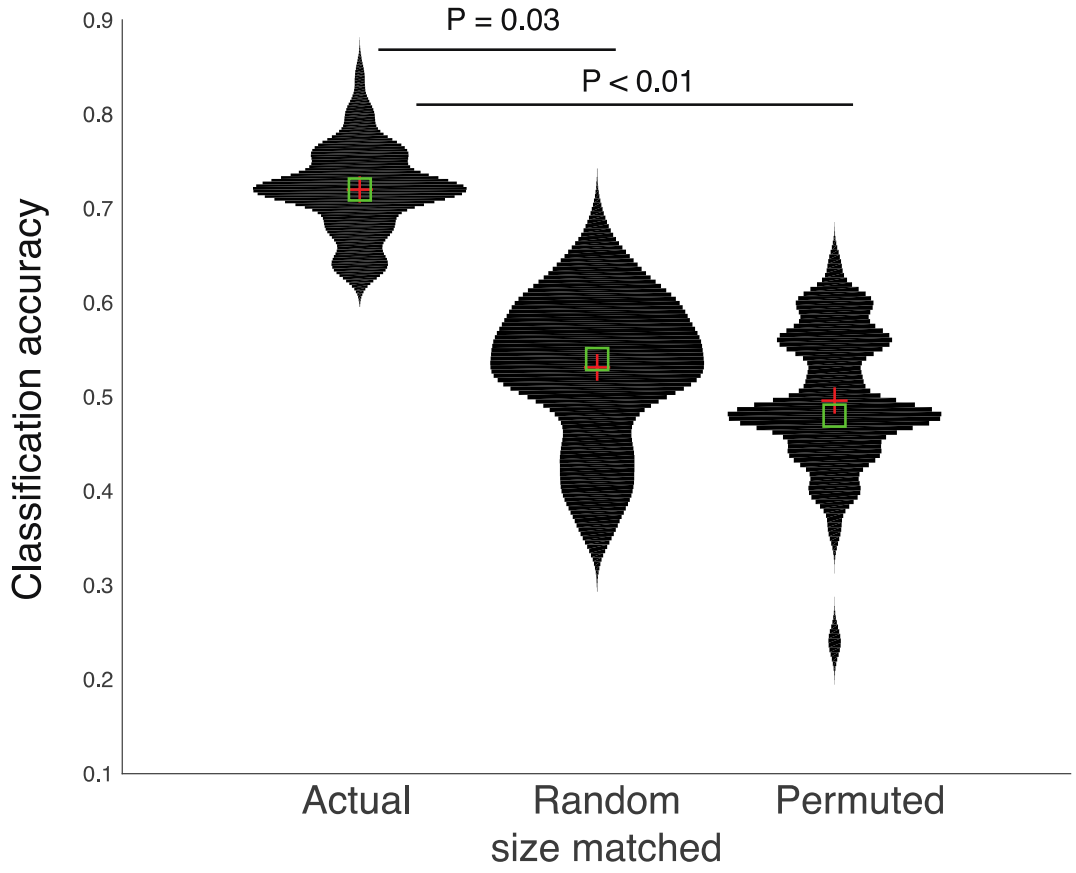

Fig. S4. Model performance in ARR vaccinees.
The violin plot shows the distribution of classification accuracies of the real model across cross-validation replicates, as measured in a tenfold cross-validation framework, compared to the classification accuracies of a model on permuted data or randomly selected data in a matched tenfold cross-validation framework for the ARR arm. The red cross and green square indicate the mean and median of the distribution, respectively. Exact P values were computed using a permutation test.

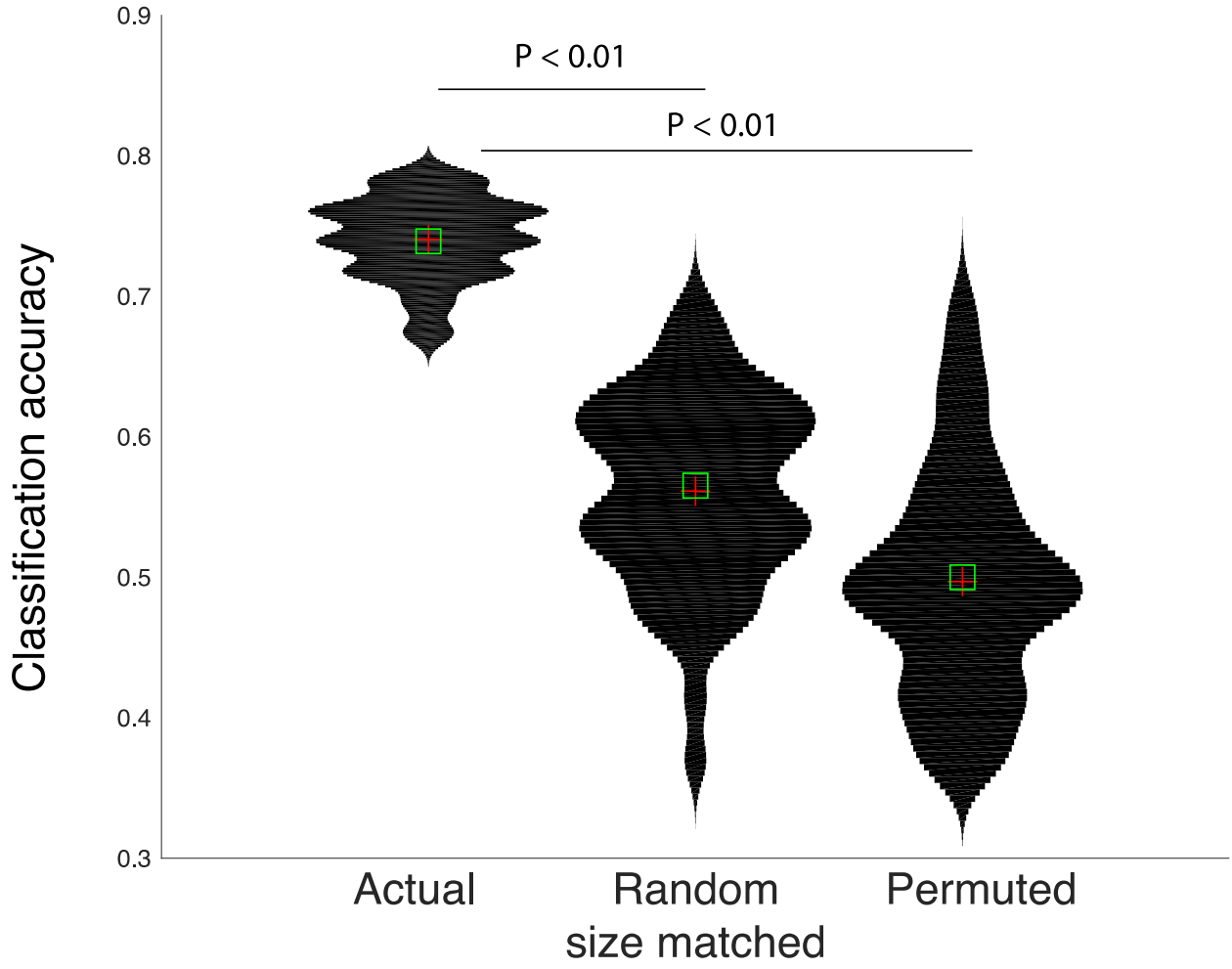

Fig. S5. Performance of model separating protected from infected vaccinees, independent of vaccine arm in the MAL068 study.
The violin plot shows the distribution of classification accuracies of the real model across cross-validation replicates, as measured in a tenfold cross-validation framework, compared to the classification accuracies of a model on permuted data or randomly selected features measured in a matched tenfold cross-validation framework. The red cross and green square indicate the mean and median of the distribution, respectively. Exact P values were computed using a permutation test.

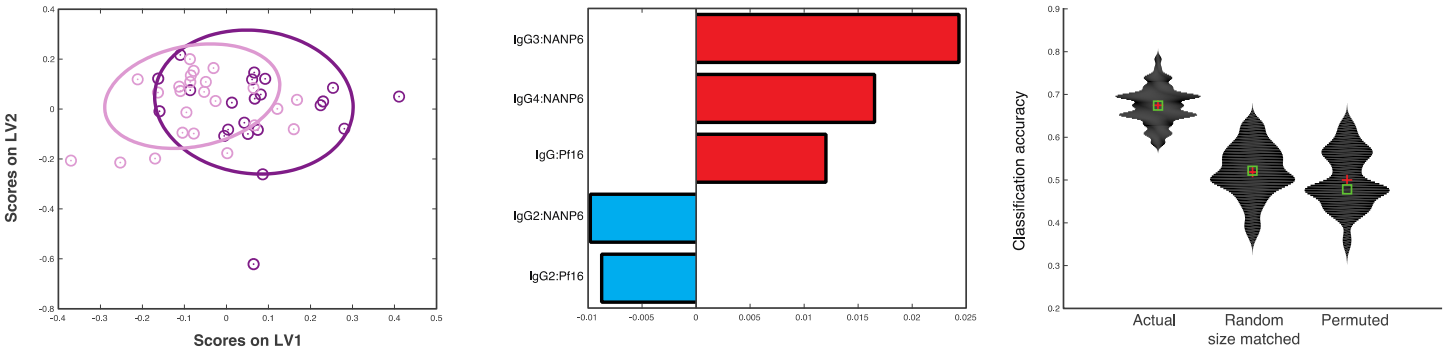

Fig. S6. Measurement of antibody concentrations alone cannot predict protection in the MAL068 study. PLS LV score biplot using CSP-, NANP6-, and Pf16-specific subclass/isotype LASSO-selected features provide minimal classification accuracy in splitting subjects based on protection status. Ellipses correspond to 75% confidence intervals for each group. The bar graph represents the PLS VIP plot corresponding to the features used to classify individuals by protection status. The violin plot shows the limited classification accuracies of the model built on subclass/isotype concentrations alone (Actual) compared to random or permuted data across cross-validation replicates, measured in a tenfold cross-validation framework.

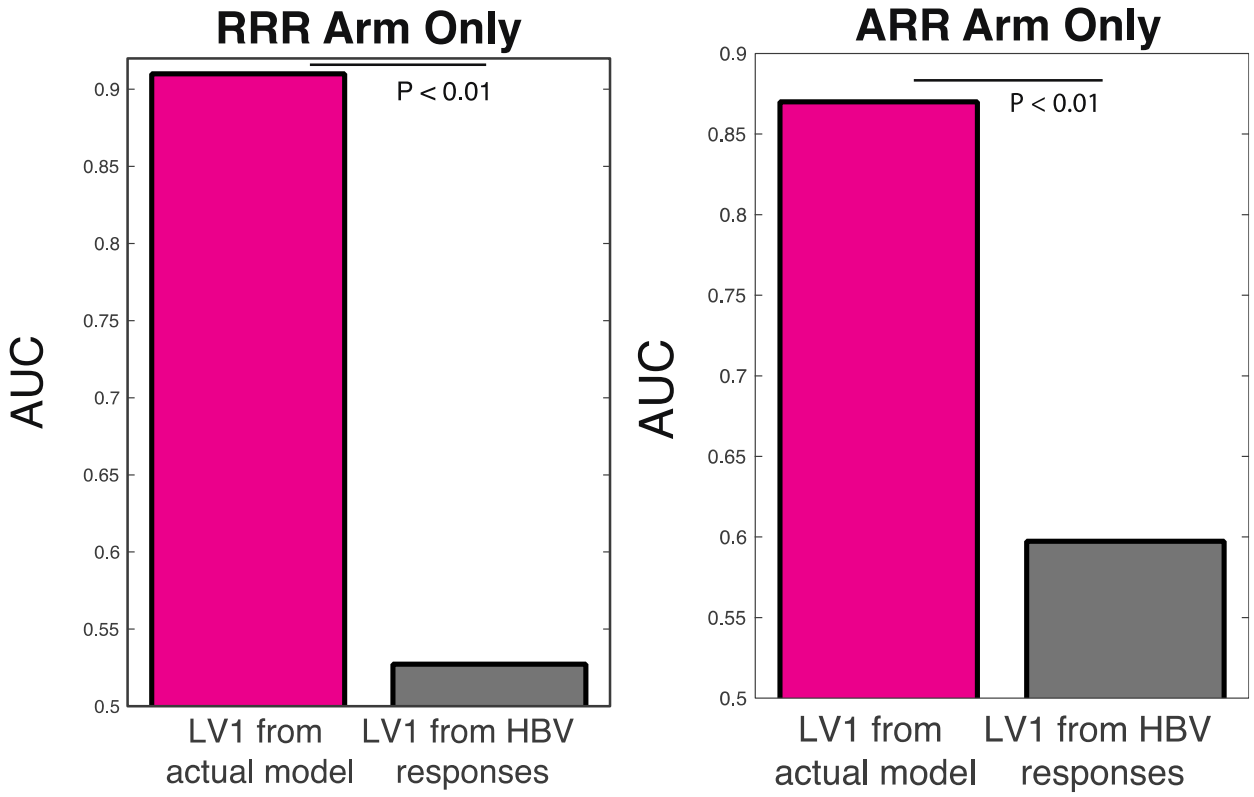

Fig. S7. Measurement of hepatitis B virus–specific antibody concentrations cannot predict protection in the MAL068 study.

The bar graphs depicts the predictive power, as quantified by AUROC, of the composite latent variable LV1, which is composed of the LASSO/PLS-selected CSP-, NANP6-, and Pf16-specific features from the MAL068 study, compared to the predictive power of a model built using HBV-specific features alone for the RRR (left) and ARR (right) arms of the MAL068 study.

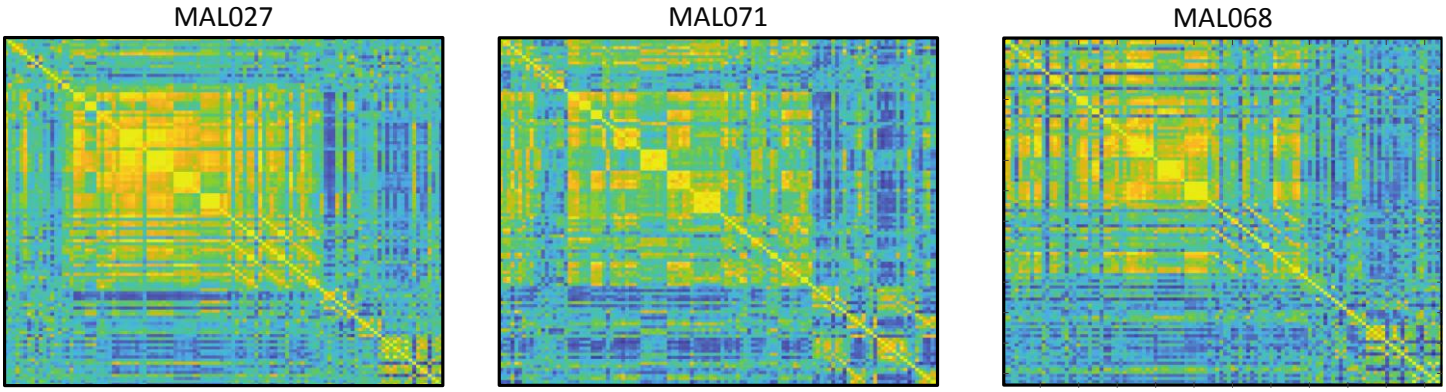

Fig. S8. Architecture of immune responses in individuals vaccinated with RTS,S/AS01 across studies. The correlation heat maps show the relationships between all features within each RRR arm in the MAL068, MAL027, and MAL071 trials. Yellow indicates positive correlations, and blue indicates negative correlations.

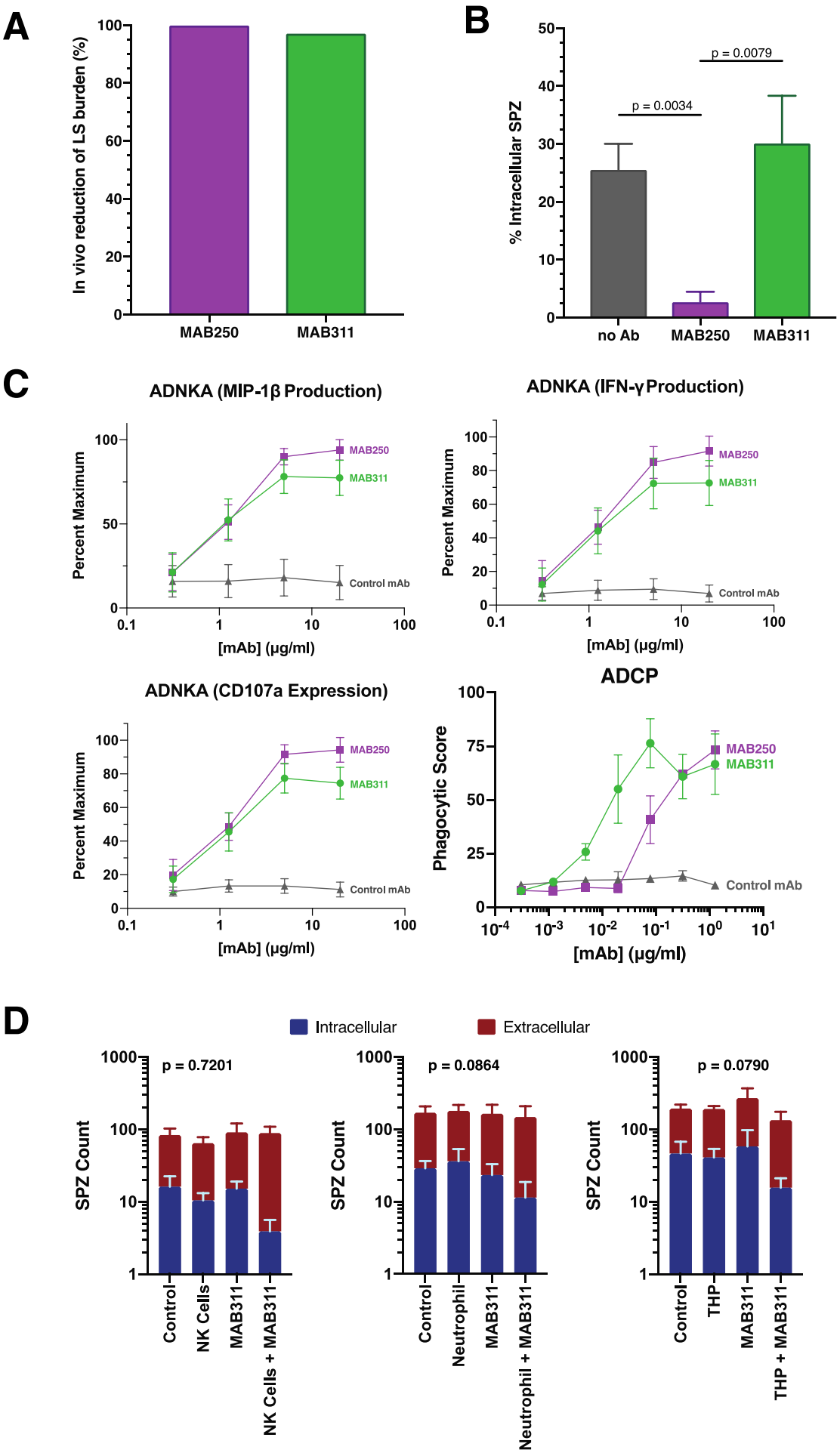
A
In vivo reduction of LS burden (%)
MAB250
MAB311
B
% Intracellular SPZ
p = 0.0034
p = 0.0079
no Ab
MAB250
MAB311
C
ADNKA (MIP-1β Production)
ADNKA (IFN-γ Production)
ADNKA (CD107a Expression)
ADCP
Percent Maximum
Phagocytic Score
[mAb] (µg/ml)
MAB250
MAB311
Control mAb
D
Intracellular
Extracellular
SPZ Count
p = 0.7201
p = 0.0864
p = 0.0790
Control
NK Cells
MAB311
NK Cells + MAB311
Neutrophil
Neutrophil + MAB311
THP
THP + MAB311

Fig. S9. In vitro and in vivo activity of CSP-specific monoclonal antibodies.
The bar graphs depict the ability of the tested monoclonal antibodies to reduce the (**A**) in vivo and (**B**) in vitro infection of hepatocytes by sporozoites. In vivo protection was assessed in mice using PfCSP-expressing *P. berghei*. In vitro inhibition of sporozoite invasion was assessed using a previously described sporozoite invasion assay and primary human hepatocytes. The line graphs (**C**) depict the ability of the tested monoclonal antibodies to activate NK cells and induce phagocytosis by THP-1 cells (ADCP). In vitro antibody-dependent NK cell activation was measured using CSP-coated plates and primary NK cells isolated from three seronegative donors; the data is presented as the average percent maximum activity observed for a specific donor. ADCP activity was measured using CSP-coated fluorescent beads. The stacked bar graphs (**D**) depict the sporozoite counts for the in vitro sporozoite restriction assays. Blue bars indicate intracellular sporozoite counts, and red bars indicate extracellular sporozoite counts. The data are presented as the mean ± 95% confidence intervals. Data were analyzed using a Mann-Whitney U-test (A–C) or a Kruskal-Wallis test (D).